Physics of the Earth and Planetary Interiors

First-principles simulations of liquid iron-heavy element alloys at high pressure

--Manuscript Draft--

Manuscript Number:	PEPI-D-22-00074R1
Article Type:	Research Paper
Keywords:	First-principles computation; liquid iron; liquid density; siderophile elements; High pressure; outer core
Corresponding Author:	Bijaya B Karki, Ph.D. Louisiana State University and A&M College: Louisiana State University Baton Rouge, LA UNITED STATES
First Author:	Dipendra Banjara
Order of Authors:	Dipendra Banjara
	Dipta B Ghosh
	Bijaya B Karki, Ph.D.
Abstract:	Iron-rich metallic liquid in the Earth's outer core is thought to contain many elements. While the incorporation of light elements in liquid iron has been widely studied, liquid iron-heavy element mixtures, particularly considering Co, Mo, and W which are relevant in constraining core-forming conditions need more studies. Here we investigate the thermodynamic and structural behavior of these siderophile elements and Ni dissolved in liquid iron in the amount of 2.67 atom% using firstprinciples molecular dynamics over the pressure range of the entire Earth's interior at temperatures 4000 to 7000 K. The calculated pressure-volume-temperature results of these iron-rich alloys are accurately described by adding the appropriative terms to the equation of state of pure iron liquid to account for the effects of temperature and impurity. The calculated mean iron coordination number of Mo and W is somewhat larger than that of Ni and Co and host iron atoms thus implying substitutional incorporation mechanism. The lack of clustering activity among the impurity atoms means that each of these impurity elements is soluble in liquid iron. Our analysis also shows that Mo and W increase the liquid density much more than Ni and Co mainly for mass reason while the bulk modulus remains essentially unaffected in all cases. The presence of heavy elements widens the apparent density gap between iron-rich liquid and the outer core so additional amounts of lighter impurity elements should be considered when constraining the core composition.
Suggested Reviewers:	Taku Tsuchiya suchiya.taku.mg@ehime-u.ac.jp
	Koichiro Umemoto umemoto@elsi.jp
	Gerd Steinle-Neumann g.steinle-neumann@uni-bayreuth.de
	Dario Alfe d.alfe@ucl.ac.uk
	Joshua Townsend jptowns@sandia.gov
	Marc Hirschmann mmh@umn.edu
Response to Reviewers:	

February 27, 2023

Dear Editor Hirose,

Please consider the revised manuscript entitled “First-principles simulations of liquid iron-heavy element alloys at high pressure” by Banjara, Ghosh, and Karki for publication in Physics and Earth and Planetary Interiors. During the revision, we have taken care of the suggestions and comments provided by both reviewers as much as we could. The revised texts are highlighted in the revised manuscript. We have also provided our point-by-point responses explaining how we have addressed the reviewers’ concerns.

We believe that our revised paper is acceptable for publication in PEPI.

Sincerely,

Bijaya B. Karki, The corresponding author
Louisiana State University, Baton Rouge, Louisiana 70803, USA
E-mail: bbkarki@lsu.edu

Point-by-point Response to Reviewers' comments and suggestions

Reviewer #1:

The authors present a first-principles molecular dynamics (FPMD) study of iron andiron-alloy liquids containing some geophysically relevant impurities. Their goal is to better understand the Earths core, which although is primarily iron, must contain other elements, too. The paper is well organized and the conclusions the authors draw are well-supported by the data they obtain from their simulations. As for their calculations themselves, they are fairly straight-forward molecular dynamics calculations using the very well-known PBE functional. The authors use their FPMD calculations on a grid of (V,T,X) points to produce an P(V,T,X) model for pure iron liquid as well as the iron alloy liquid. The approach and results are well-within the area of interest to the PEPI readership, and I think the paper should be considered for publication after consideration of the following relatively minor suggestions and clarifications are made.

Response. We thank the reviewer for recognizing the importance of our work and for offering several suggestions and comments.

1.) In Fig. 8, the shock data from Anderson and Ahrens is shown, but it isn't clear how well the authors FPMD results compare. Have the authors considered including an estimate of the principal Hugoniot obtained from their EOS model? This might be a cleaner way to compare to the shock data.

Response. We did not try to obtain the principal Hugoniot. As emphasized in the paper, we compared our calculated results only with static compression data from the diffuse scattering experiments (Kuwayama et al., 2020) to obtain the empirical correction term. Since temperature in the shock-wave experiments is model dependent, we did not consider the comparison with the shock-wave data unlike some previous studies.

2.) The authors state that including the Hubbard +U term in their calculations generally resulted in a worse EOS model, in the sense that the V0 term showed a larger disagreement with experiment. It was hard for me to make sense of this result. Naively, I would have anticipated that the dense liquid structure, for example, might be rather sensitive to the treatment of the d-electrons, as just one example. Unfortunately, not much details are given about how those calculations were performed. Therefore, it was hard to weigh the conclusions the authors drew. It would be valuable, for example, to know whether the +U was added only to the Fe, or to Ni, Cr, and W as well? And how was the value of +U chosen? Famously, there are many metastable states within the +U approach, so how did the authors ensure that they obtained reliable results?

Response. We agree with the reviewer that the use of the Hubbard +U term is not easy. It may not be good idea to assess its effects on EOS based on a couple of simulation runs. We decided to delete the relevant sentence from the main text.

3.) Similarly, how was spin treated in the calculations generally, and especially with the +U calculations?

Response. We did not consider spin in our simulation like most previous computational studies of pure iron and its alloys. Considering the spin effects and the use of Hubbard +U term will involve many more simulations, which is beyond the scope of this study.

4.) The authors explored only very small defect concentrations (<3 atom%), and derive a polynomial compositional term to include in their EOS model. Do the authors expect that this model will be reasonably accurate for larger impurity concentrations?

Response. The model for the impurity pressure term is expected to work for small to moderate concentrations, which are of relevance for the core composition. We have found that the model obtained by using 2.67 atom% data reproduces well the pressure results for 5.33 atom% of W. Please see new supplementary figure Fig. S1, which displays the calculated results for FeW liquid for two concentrations: 2.67 and 5.33 atom% of W.

Reviewer #2:

In this work, the authors use first-principles calculations to study liquid iron alloys FeX (X = heavy elements Ni, Co, Mo, and W) at the Earth's core condition. The EoS, heat capacity (Cv) and Gruneisen parameter (gamma) of these liquid FeX alloys are obtained. The authors also studied the structural properties of FeX alloys, showing that the heavy elements X can be dissolved into iron liquid by substitution without clustering and thus increase the density of the liquid. These results suggest that metallic droplets containing heavy elements may have sunk to the core during the Earth's core-mantle differentiation.

Overall, the results presented in this manuscript are of interest to the readership of PEPI, the calculations and analysis seem fine, and the writing is clear. I therefore recommend this manuscript for publication in PEPI after some revisions, as described below.

Response. We thank the reviewer for pointing out the importance of our results and for providing us with constructive comments.

(1) I find the description of Fig. 2A unclear. Are all the crossing symbols the same kind of FeX alloys or not? I guess it's on the Fe-Mo alloy? It is neither described in the text nor in the caption.

Response. We revised the figure caption to avoid the confusion. The open symbols represent pure liquid iron and small solid spheres represent all four alloys.

(2) In Fig. 4, the authors plot Cv and gamma for Fe and FeX. For Fe, Cv and gamma at T = 2500 and 3500 are plotted. For FeX, however, only the "average between 4000 and 7000 K" are plotted. I am wondering why the authors chose the "average" all these results instead of plotting the at several different T. If the results at T= 4000 and 7000 K are highly close, the authors should plot that in the figure or at least mention that in the main text.

Response. Yes, the Cv and gamma results at T = 4000 to 7000 K are close to each other, so we prefer to show the average values for the sake of clarity. We have added a supplementary figure Fig. S3which show the results at all temperatures for the case of pure iron liquid.

(3) Following the above comment, I am also wondering why the authors only show the calculated raw data in Fig. 4 without showing a smooth curve of isothermal Cv(V) and gamma (V) at a several T. The authors already obtain a modeled V(P,T) and/or P(V,T) relations in Eqs. 1-4 for these Fe X alloys. From there, free energy F(V,T) and G(P,T) can in principles be obtained, so Cv and gamma can be obtained. By plotting the modeled results along with the DFT data can really showcase how good the proposed model really is.

Response. The values of Cv and gamma were calculated directly from the pressure-energy results obtained from the simulations at different temperatures for each volume. We evaluated dE/dT or dP/dT at each volume by taking the differences between energies or pressure at two successive temperatures. This way the calculated values of Cv and gamma will not be affected by the forms of the EoS we used.

(4) I find the caption of Fig. 5 confusing. The last sentence reads "Note that the partial Fe-Fe curve of each alloy liquid (not shown here) almost overlaps with the Fe-Fe curve of pure liquid iron." I am wondering what "partial Fe-Fe curve of each alloy" is, and how the readers can see something not shown in the figure to overlap with the curve shown in the figure.

Response. We added a supplementary figure Fig. S6 comparing Fe-Fe RDFs of four alloy liquids with Fe-Fe of pure iron liquid. The curves are indistinguishable from each other.

(5) As indicated in Fig. 5, the RDF curves of Ni-Fe and Co-Fe show greater resemblance to the Fe-Fe curve, while Mo-Fe and W-Fe significantly deviate from Fe-Fe. The authors should explain in more detail and offer more insights for this phenomenon rather than simply reporting it.

Response. We added some explanation in relation to the different atomic sizes. Ni and Co have similar radii as iron atoms whereas Mo and W atoms are larger.

(6) For Fig. 6, same as my comments for Fig. 5. The authors should explain in more detail why Mo-Fe and W-Fe alloys behave this way.

Response. Again, this appears to be the similar size of Mo and W atoms as discussed in the paper.

(7) Densities of liquid Fe and FeX alloys are the main topic of this manuscript. I therefore encourage the authors to include both Figs. 8 and S5 in the main text and incorporate these two figures into their discussion in the main text.

Response. Following this suggestion, we have moved Fig. S5 to the main text as Fig. 9 and talked about the density results of all alloys.

(8) At the end of Sec. 4, the authors point out that Fe-Mo and Fe-W may have sunk to the during the core-mantle differentiation. Can the authors further elaborate the geophysical importance of this in the same Section?

Response. We have elaborated this inference a bit more in the main text.

(9) Based on Fig. 4B, FeX alloys at high pressure (small V/Vo), especially Fe-W and Fe-Mo, have a smaller gamma than pure Fe. Considering Fe-W and Fe-Mo may have sunk to the core during the core-mantle differentiation, would this smaller gamma have some possible geophysical effects? Can the authors make some comments?

Response. While the differences in gamma in the presence of heavy elements are noticeable, they are fairly small. In general, smaller gamma values at higher pressure imply a smaller temperature gradient in the deeper parts of the outer core. The presence of impurity tends to slow down temperature increase across the outer core.

First-principles simulations of liquid iron-heavy element alloys at high pressure

Dipendra Banjara[a], Dipta B Ghosh[a,b] and Bijaya B Karki[a,b,c,*]

[a]*School of Electrical Engineering and Computer Science*, [b]*Department of Geology and Geophysics*, [c]*Center for Computation and Technology, Louisiana State University, Baton Rouge, LA 70803, USA*

[*]Corresponding author: bbkarki@lsu.edu (B.B. Karki)

ABSTRACT

Iron-rich metallic liquid in the Earth's outer core is thought to contain many elements. While the incorporation of light elements in liquid iron has been widely studied, liquid iron-heavy element mixtures, particularly considering Co, Mo, and W which are relevant in constraining core-forming conditions need more studies. Here we investigate the thermodynamic and structural behavior of these siderophile elements and Ni dissolved in liquid iron in the amount of 2.67 atom% using first-principles molecular dynamics over the pressure range of the entire Earth's interior at temperatures 4000 to 7000 K. The calculated pressure-volume-temperature results of these iron-rich alloys are accurately described by adding the appropriative terms to the equation of state of pure iron liquid to account for the effects of temperature and impurity. The calculated mean iron coordination number of Mo and W is somewhat larger than that of Ni and Co and host iron atoms thus implying substitutional incorporation mechanism. The lack of clustering activity among the impurity atoms means that each of these impurity elements is soluble in liquid iron. Our analysis also shows that Mo and W increase the liquid density much more than Ni and Co mainly for mass reason while the bulk modulus remains essentially unaffected in all cases. The presence of heavy elements widens the apparent density gap between iron-rich liquid and the outer core so additional amounts of lighter impurity elements should be considered when constraining the core composition.

1. Introduction

Iron is considered as the main constituent of the Earth's core. Molten iron shows large density (8 - 10%) and velocity (4-5%) differences with respect to the outer liquid core (e.g., Anderson and Ahrens, 1994; Alfe et al., 2000; Ichikawa et al., 2014; Kuwayama et al., 2020). Therefore, light elements, such as H, C, N, O, S, etc. must be incorporated in liquid iron to explain the discrepancy (e.g., Poirier, 1995; Morard et al., 2013; Badro et al., 2014; Tagawa et al., 2021). Any volatile impurities not only lower the density of liquid iron-rich alloy but also raise its bulk sound velocity to make these properties comparable to the seismic profiles of the outer core. They also lower the melting temperature of iron and thus help the outer core remain in the liquid state (Sakamaki et al. 2008; Fei and Brosh, 2014)). Under inner core conditions, the light elements are also incorporated in solid iron though in lesser amounts because of smaller density deficit.

Based on geochemical, cosmological, and meteoritical arguments, the composition of the outer core perhaps is even more complex (McDonough and Sun, 1995; Hirose et al., 2013). During the core formation by accretion of planetary embryos and impacting planetesimals, siderophile elements could have disproportionately partitioned into the metallic core while lithophile elements were left behind in the silicate mantle. For instance, refractory siderophile elements, including Ni, Co, Mo, and W may have been swept down into the core with molten iron in significant amounts. Nickel is present in liquid iron in several percent (~5%) while Co, Mo, and W are present in much smaller amounts (less than 1% together). Despite their small amounts, Co, Mo, and W are considered to serve as important tracers for the conditions and timing of core formation (e.g., Rubie et al., 2003; Fischer et al., 2015; Huang et al., 2021). How these geochemically significant elements behave in liquid iron and how they influence host properties help us better understand the formation and evolution of the core.

Iron-rich liquids have been studied extensively under varying conditions of pressure and temperature using both computational and experimental methods. First-principles computational approach has so far focused on pure iron liquid (Alfe et al., 2000; Ichikawa et al., 2014) and iron-light element mixtures (Badro et al., 2014; Umemoto and Hirose, 2015; Ichikawa and Tsuchiya, 2020; Bajgain et al., 2021) with the aim of constraining the concentration of each alloying element that can match the seismic density and velocity profiles of the outer core. These computations have investigated the equation of state, structure, and diffusivity of binary iron-rich and some Fe-Ni ternary systems. Such studies are not yet done in the context of liquid iron-heavy element mixtures considering Co, Mo, and W. On the other hand, experiments have investigated a wide range of properties, including density and metal-silicate partitioning, but they are generally confined to relatively narrow pressure and temperature conditions (Fisher et al., 2015; Huang et al., 2021; Tagawa et al., 2021). A recent experimental study of pure liquid iron has reported the density up to 116 GPa and 4350 K by diffuse x-ray scattering and the bulk sound velocity up to 46 GPa and 2700 K by inelastic x-ray scattering (Kuwayama et al., 2020). These data complement the shock-

wave data at 278-397 GPa (Brown and McQueen, 1986; Anderson and Ahrens, 1994). Thus, the density data are still not available at almost all conditions of the outer core.

Here we report a first-principles study of four iron-rich liquid alloys considering heavy elements, including Ni, Co, Mo, and W. While FeNi liquid was previously simulated (Posner and Steinle-Neumann, 2019; Umemoto and Hirose, 2020; Ichikawa and Tsuchiya, 2020), the computational study of Co, Mo, and W-bearing iron alloy liquids is still lacking. Our focus is on the equation of state and structural behavior of these four alloys in comparison to the pure iron liquid at pressures up to 380 GPa and temperatures up to 7000 K thus covering the pressure-temperature conditions of the entire earth's interior. We also present implications of our structural and density results for the outer core and core formation.

2. Methods

First-principles molecular dynamics (FPMD) simulations were performed within the generalized gradient approximation (GGA) and projector augmented wave formalism using VASP - Vienna ab initio simulation package (Kresse and Furthmüller, 1996). The GGA functional used was Perdew-Burke-Ernzerhof type as in most previous computational studies (Perdew et al., 1996). The gamma point was used for Brillouin zone sampling and the energy cutoff of 400 eV was used for plane wave basis set.

The simulation supercell consisted of 150 atoms for pure iron liquid (Fe_{150}). To simulate each FeX system where X = Ni, Co, Mo, and W, four randomly selected iron atoms in the liquid iron supercell were replaced with the respective alloying element. We thus generated four independent supercells with compositions $Fe_{146}Ni_4$, $Fe_{146}Co_4$, $Fe_{146}Mo_4$, and $Fe_{146}W_4$, each of which corresponds to an impurity concentration of 2.67 atom%. In the case of W-bearing alloy, we also considered a higher concentration of 5.33 atom% by using $Fe_{142}W_8$ supercell. Our FPMD simulations were based on the canonical *N*-*V*-*T* ensemble with Nose thermostat, where *N* is the number of atoms, *V* is the volume, and *T* is the temperature. The initial structure for pure iron was melted at 8,000 K (or higher temperature for small volumes) and then quenched down to desired lower temperatures. Depending on temperature, different volume ranges between $V/V_0 = 1.06$ and 0.59 (where $V_0 = 1728.0$ Å^3 was used as a reference volume) were considered. At each thermodynamic state considered, the total pressure (*P*) represents the sum of the pressure obtained from the FPMD simulation, the ideal gas contribution given by NkT/V (where *k* is Boltzmann constant) and small Pulay stress of 0.4 to 0.8 GPa over the volume range considered. The run durations of our simulations ranged from 10 picoseconds at 7000 K to 20 picoseconds at 4000 K with a time step of 1 fs. For pure liquid iron, we also considered 2000 and 3000 K isotherms and additional volumes to cover the conditions at which experimental data are available for comparison (Kuwayama et al., 2020). A few simulations were performed along the 4000 K isotherm using the local density approximation to the exchange-correlation functional. For each simulated system, we

used the atomic-position time series to analyze local structure and speciation of the impurity elements. Selected simulations were run much longer to ensure that the calculated properties were well converged.

3. Results and Analysis

3.1 Equation of state

We first present and analyze the calculated pressure-volume-temperature results of pure iron liquid shown in Fig. 1. The pressure varies from 1.0 to 11.8 GPa at 2000 K, 1.9 to 90.3 GPa at 3000 K, 9.0 to 140.6 GPa at 4000 K, 15.5 to 270.0 GPa at 5000 K, 21.6 to 368.7 GPa at 6000 K, and 130.5 to 380.4 GPa at 7000 K for the respective volume ranges considered. These results are accurately described using the following relation:

$$P(V,T) = P(V,T_0) + B_{\text{th}}\,(T\text{-}T_0) \qquad (1)$$

Here the reference isotherm T_0 = 5000 K (first term) is described by the fourth-order Birch-Murnaghan equation of state with V_0 = 1728.0 Å^3 which corresponds to P_0 = 25.6 ± 0.3 GPa at 5000 K (shown by the black curve and circles in Fig. 1). The fit parameters are: K_0 = 196.2 ± 0.3 GPa, K_0' = 4.51 ± 0.06, and K_0'' = -0.026 ± 0.002 GPa^{-1}.

The thermal pressure P_{th} term contains the volume-temperature dependent coefficient:

$$B_{\text{th}}(V,T) = \left[0.0203 - 0.0132\left(\frac{V}{V_0}\right)\right]\left[0.9 + 0.1\left(\frac{T_0}{T}\right)\right] \qquad (2)$$

in the units of GPaK^{-1}. The model $P_{\text{th}} = B_{\text{th}}\,(T\text{-}T_0)$ describes well the values of thermal pressure calculated relative to 5000 K as a function of compression at different temperatures for pure and alloyed iron liquids (Fig. 2A). The two-term form of the equation of state (Eq. 1) gives root mean square error of 0.35 GPa for pure iron liquid thereby giving accurate representation over very wide ranges of pressure (0 to 400 GPa) and temperature (2000 to 7000 K).

We find that at the same volume and temperature conditions the calculated pressures for Ni- and Co-bearing liquids almost overlap with those for pure iron liquid lying within 0.8 GPa. However, the addition of Mo or W to liquid iron gives systematically higher pressure. The impurity-induced change in the pressure increases from about 2 to 17 GPa for Mo/W-bearing liquids over two-fold compression range considered (Fig. 2B). This finding is generally consistent with the notion that both Mo and W have larger atomic radii than iron radius. By adding an impurity-dependent term, we obtain the equation of state for iron-rich liquids as follows:

$$P(V,T) = P(V,T_0) + B_{\text{th}}\,(T\text{-}T_0) + B_{\text{im}}\,x \qquad (3)$$

Here x is the impurity concentration in atom% (equivalently, mol%) of iron-rich binary alloy liquid and B_{im} is a volume-dependent coefficient expressed as

$$B_{\mathrm{im}}(V) = a + b\left(\frac{V}{V_0}\right) + c\left(\frac{V}{V_0}\right)^2 \quad (4)$$

in the units of GPa per atom%. The parameters a, b, and c take small values, respectively, -0.13, 0.27, and 0 for $Fe_{146}Ni_4$ and -0.30, 0.42. and 0 for $F_{146}eCo_4$ liquid. Their respective values are 22.8, 40.8, and 18.8 for $Fe_{146}Mo_4$ and 27.1, -48.7, and 22.5 for $Fe_{146}W_4$ liquid. We find that the model $P_{\mathrm{im}} = B_{\mathrm{im}}\, x$ adequately describes the impurity-induced pressure values relative to pure iron liquid for x = 2.67 atom% (Fig. 2B). The model also works well for higher concentration as shown for the case of 5.33 atom% W-bearing iron liquid (Fig. S1). It is remarkable that the proposed three-term form of the equation of state (Eq. 3) accurately represents the calculated pressure-volume-temperature results for all iron-rich alloy systems (Fig. 3). The root mean square errors are 0.34, 0.29, 0.41, and 0.60 GPa, respectively, for Ni-, Co-, Mo- and W-bearing liquids. We find that the bulk modulus of iron-rich liquid remains essentially unchanged in the presence of any of these heavy elements (Fig. S2).

From the calculated temperature variations of the energy and pressure, we evaluate the heat capacity at constant volume and the thermal Grüneisen parameter using $C_V = \left(\frac{dE}{dT}\right)_V$ and $\gamma = \left(\frac{V}{C_V}\right)\left(\frac{dP}{dT}\right)_V$, respectively. Both C_V and γ are highly sensitive to pressure and some extent to temperature. The value of specific heat evaluated by assuming the linear temperature variation of energy at each volume in the range 4000 to 7000 K is constant with respect to temperature, but its value increases with compression (Fig. 4A). On the other hand, the value of γ evaluated assuming the linear temperature variation of thermal pressure at each volume in the same temperature range tends to increase somewhat initially with compression and then gradually decreases at higher pressures (Fig. 4B). The predicted behavior of C_V and γ is generally consistent with the previous calculations of iron liquid at high temperatures (Alfe et al., 2000; Bajgain et al., 2021). The calculated constant-temperature values of C_V and γ for all four alloys almost overlap with those of pure liquid iron (Fig. 4A, B). Thus, both thermodynamic parameters are essentially insensitive to the composition of iron-rich liquid for small impurity concentrations considered in this study (Fig. S1). Assuming a non-linear temperature variation for both energy and thermal pressure, we find that C_V does not show any systematic trend with temperature but γ slightly increases with deceasing temperature from 6500 K to 4500 K (Fig S3). They tend to take larger values as temperature is lowered further. For instance, the reference volume values of γ are 1.79 at 3500 K and 1.96 at 2500 K compared to the high-temperature average of 1.57. For pure and all iron alloy liquids, we generally find smaller gamma values at higher pressure (Fig. 4B). This implies a smaller temperature gradient in the deeper parts of the outer core.

3.2 Structural Properties

We analyze the structural properties of pure and alloyed iron liquids in terms of radial distribution functions and coordination environments. For pure iron liquid, the radial distribution

function shows characteristic features of a simple monoatomic liquid at all conditions (Fig. 5A and B). The calculated Fe-Fe RDF at low pressure shows a clear first peak at about 2.4 $Å^3$ corresponding to short-range order and subsequent smaller and broader peaks eventually converging to the unity implying the absence of long-range order. The first peak gets shorter and broader with increasing temperature whereas it becomes taller and sharper with increasing pressure (Fig. S4). The positions of both the first peak and the first minimum shift to shorter distance by about 0.3 and 0.5 Å, respectively, as the liquid is compressed from V/V_0 = 1.06 to 0.59 (Fig. S4). The predicted pressure-induced shifts are qualitatively consistent with the recent experimental inferences (Kuwayama et al., 2020).

For binary $Fe_{146}X_4$ liquids, we consider three partial radial distribution functions corresponding to the Fe-Fe, Fe-X, and X-X correlations. Irrespective of impurity type (X = Ni, Co, Mo, or W), the Fe-Fe RDF of all alloy liquids shows a well-defined peak which essentially overlaps with that of pure iron at all conditions. The X-Fe (equivalently, Fe-X) functions also show a clear first peak which is sensitive to both temperature and pressure. It is interesting to note that the Ni-Fe and Co-Fe functions closely resemble the Fe-Fe RDF with their first peaks almost overlapping with each other at all conditions (Fig. 5A). This means that both Co and Ni structurally behave as host iron atoms and can be considered iron-like as suggested previously for Ni-bearing iron alloy (Posner and Steinle- Neumann, 2019; Umemoto and Hirose, 2020). On the other hand, the Mo-Fe and W-Fe peaks are shifted to the right by about 0.2 Å (Fig. 5B). At a constant volume, the first peak of each X-Fe RDF becomes shorter and broader with its position shifting to shorter distance as temperature increased. Along a given isotherm, the peak becomes taller and sharper and systematically shifts to shorter distance as the liquid is compressed (Fig. S5). The minimum after the first peak gets deeper and shifts to shorter distance with compression but does not change noticeably with temperature. We find that the X-X RDF of each alloy liquid shows a weak peak at most conditions implying weak impurity-impurity correlation, so no direct bonds are formed among the impurity atoms (Fig S5). However, the Fe-Fe RDF of alloy liquid remains essentially unaffected by in the presence of the impurity element (Fig S6).

We calculate the average lengths of Fe-Fe and X-Fe (or Fe-X) bonds in all liquids from the first peak of the corresponding RDFs as a function of pressure and temperature. The average Fe-Fe distance is not affected significantly by the impurity at all conditions (Fig S7) as expected because of almost unaltered Fe-Fe RDF peak of each iron-rich alloy (Fig S6). The calculated average Ni-Fe and Co-Fe bond distances tend to be slightly larger (< 1%) than the Fe-Fe bond distance (Fig. 6). This prediction is consistent with the previous computational study of Ni-bearing liquid (Posner and Steinle-Neumann, 2019). In contrast, both Mo-Fe and W-Fe bonds are longer than Fe-Fe bonds by about 5 and 6%, respectively (Fig. 6). Wider RDF peaks and corresponding longer bond distances of Mo and W-bearing alloys can be related to the notion that Mo and W atomic radii are larger than the atomic radius of host iron, which is comparable to the radii of Ni and Co atoms.

For pure iron liquid, we examine local coordination environment involving multiple atoms which are the nearest neighbors of each atom. The mean Fe-Fe coordination number (Z_{FeFe}) is calculated by counting those iron atoms which lie within the cutoff distance corresponding to the minimum after the first peak of the radial distribution function. The calculated value of Z_{FeFe} is around 12.8 at low pressures and it tends to increase somewhat initially with compression and always remains below 13.5 at pressures up to ~400 GPa (Fig. 7A). The effects of temperature on coordination are small and do not show any discernable trend. Considering all thermodynamic states, we find that the mean Fe-Fe coordination number of liquid iron is somewhat larger than the coordination number of 12 for the cubic and hexagonal close-packed structures of solid iron. The liquid iron thus adopts a very dense structure of packing. At each condition, the coordination environment exhibits broad distribution consisting of 8-fold to 15-fold states in different proportions. As pressure increases, the coordination distribution shifts to higher values with increased proportions of 14 and 15-fold states at the expense of low coordination species (8- and 9-fold). The absence of low coordination states (below 8-fold) means that directional bonding is essentially absent in the liquid structure of iron.

We can define four types of coordination numbers for FeX alloy liquid: Z_{FeFe}, Z_{XFe}, Z_{FeX}, and Z_{XX}. Each alloying element tends to suppress the coordination among host iron atoms at all conditions. The reductions in Z_{FeFe} compared to pure liquid iron are in the range 2 to 4% for each binary iron alloy containing 2.67 atom % impurity (Fig. 7A). This means that the host atoms are also coordinated with some impurity atoms as first-nearest neighbors. All Fe-X coordination numbers are small (with Z_{FeX} taking values in the range 0.3 and 0.4) because majority iron atoms (~70%) are not bonded with any impurity atoms for the concentration considered here. The remaining Fe atoms are singly coordinated with X atoms, and the X-Fe-X connections occur in small proportion (below 5%). The sum of Z_{FeFe} and Z_{FeX} of each alloy liquid is almost equal to Z_{FeFe} of pure liquid iron.

The value of Z_{XFe} is sensitive to the type of alloying element (Fig. 7B). The mean iron coordination numbers of Ni and Co are the same as Z_{FeFe} of the alloy liquids but smaller than that of pure iron liquid. However, both Mo and W show higher Fe coordination with Z_{MoFe} and Z_{WFe} taking values between 13.5 and 15.0. The high mean Mo/W-Fe coordination numbers are consistent with longer Mo/W-Fe distances compared to Fe-Fe bonds. It is interesting to note that Z_{XFe} does not vary smoothly with compression. When the X-Fe coordination takes relatively small or large number, the impurity atoms tend to be correspondingly more or less correlated with each other. Unlike other types of coordination, we cannot define the X-X coordination precisely because of weak or no peak in the X-X RDFs. Using the respective X-Fe cutoff distances instead, we estimate Z_{XX} to lie between 0 and 1 considering all alloy liquids and all conditions. For instance, along the 5000 K, Z_{CoCo} = 0.8 and 0.0, respectively, when Z_{CoFe} is 12.5 and 13.4 so the total coordination number ($Z_{CoFe} + Z_{CoCo}$) of Co remains almost the same (13.3 and 13.4).

4. Discussion and implications

Our simulation of pure liquid iron covers the pressure range from 0 GPa at 2000 K to 380 GPa at 7000 K (Fig. 1). These results perhaps represent one of the most extensive studies of liquid iron when compared to many previous computational studies (e.g., Alfe et al., 2000; Ichikawa et al., 2014; Wagle and Steinle-Neumann, 2019; Umemoto and Hirose, 2020; Bajgain et al., 2021) and they are expected to give additional insight onto the thermodynamic behavior of liquid iron. Unlike the case of silicate melts (e.g., Karki et al., 2018), the first-principles computations tend to overestimate the liquid iron density (or underestimate the volume) considerably even with the use of GGA. As such, the differences between the calculated and experimental values of liquid iron density are large as previously noted by most previous computational studies. Accurate evaluation of the liquid density is needed to infer meaningful constraints on the composition of the Earth's outer core from density comparisons between iron-rich alloys and seismological observations. Towards this endeavor, appropriate corrections need to be made to the calculated results by considering their systematic offset from the available experimental data. We find that the calculated densities of liquid iron are higher than the measured data at zero pressure and all elevated pressures up to 116 GPa in the temperature range 1800 to 4350 K of the experimentation (Kuwayama et al., 2020). This apparent overestimation of the density by our first-principles computation ($\Delta\rho = \rho_{\text{calc}} - \rho_{\text{expt}}$) is ~1.1 g/cc at zero pressure and 2000 K. The value of $\Delta\rho$ decreases with increasing pressure to about 0.4 g/cc around 110 GPa and 4300 K. These density differences correspond to finite differences in pressure between computation and experiments as GGA systematically underestimates the pressure. Comparison with the shock-wave density data available at pressures above 270 GPa does not seem to be appropriate in this regard because temperature in the shock-wave experiments is model dependent (Anderson and Ahrens, 1994). So, we use the experimental data at pressures 0 to 116 GPa only as the reference to derive an empirical pressure correction term as a function of compression (Inset of Fig. 8):

$$P_{\text{emp}}(V) = P_{\text{expt}}(V) - P_{\text{calc}}(V) = 27 - 12\left(\frac{V}{V_0}\right) \quad (5)$$

This pressure correction is generally consistent with the previous corrections based on thermodynamics using the differences in both pressure and bulk modulus at zero pressure between computations and experiments (Wagle and Steinle-Neumann, 2019; Bajgain et al., 2021). Our correction model which is based on direct comparisons with the measured data at zero and elevated pressures is expected to be widely applicable than previous models. We find that using the local density approximation (LDA) further underestimates the pressure (Fig. 1) thus requiring even larger correction to the pressure.

The derived density-pressure profiles of pure liquid iron with the corrected pressure along all high-temperature isotherms (Fig. 8) lie systematically above the seismic density profile of the core (Dziewonski and Anderson, 1981). We also calculated the density profile along the isentropic temperature profile given by Kuwayama et al. (2020) with the inner core boundary temperature constrained at 5800 K (Fig. 8). It is thus clear that liquid iron is too dense for the outer core

composition. This notion has been established based on numerous experimental and computational studies, but the size of the density gap (or density deficient) is not well constrained. Based on our corrected equation of state, the density gap varies from 0.68 to 0.82 g/cc (that is, 6.9 to 6.7%) from the top to the bottom of the outer core, which are smaller than most previous estimates by 1 to 2% and comparable to the most recent inferences (Kuwayama et al., 2020). Based on the calculated density results (Fig. 9), the addition of Ni and Co in a few atom% does not change the density of iron-rich liquids at all. As such, these elements are invisible in the outer core with respect to the seismic density and velocity observations. However, other two heavy elements, particularly W, in any amounts tends to increase the density of iron-rich liquid (Fig. 9) thereby widening the density gap. For instance, the addition of 0.1 atom% of W increases the liquid density by ~0.02 g/cc which can be offset by the addition of about 10 times more hydrogen. This means that the estimation of the amounts of light elements in the outer core also depends on the presence of heavy elements even in fairly small amounts.

Our structural analysis shows that each of impurity elements (Ni, Co, Mo, and W) is incorporated in the liquid iron by substitutional mechanism. These impurity atoms adopt similar local structures like host iron atoms thereby taking close-pack positions. Moreover, visualization of the position-time series data reveals the presence of only transient structures consisting of two or rarely three impurity atoms bonded together. This means that the impurity atoms are less likely to form large clusters to be exsolved but instead they are compatible in the liquid iron by preferably bonding with the host atoms. We argue that iron-rich metallic liquid can dissolve any of these impurity elements in significant amounts under the pressure-temperature conditions that are relevant to the core formation time and to the present core. In the core formation model based on accreting impacting planetesimals, the iron-rich metal in each impactor may have interacted with the magma ocean and been molten (Wood et al., 2006). Metallic droplets from those impactors sank through the silicate magma ocean and siderophile elements could have then been carried down into the core along as the dissolved components (Kleine et al., 2002; Rubie et al., 2003). The amount of these elements carried to the core depends on their partitioning coefficients between the metallic liquid and silicate melts, and their diffusion rates. Our finding of structural similarity in the speciation of Mo and W in liquid iron supports the notion that these refractory siderophile elements show similar partitioning behavior (Huang et al., 2021). In the early stages of the Earth's core-mantle differentiation, these elements could have segregated to metallic liquid droplets. Such Mo- and W-bearing droplets (and metallic diapirs in the later stages) being excessively heavy could have sunk to the core. It is thus possible that the heavy elements may have been mostly collected to the bottommost part (referred to as the F-layer) which is distinct from the rest of the outer core (Zou et al., 2008).

5. Conclusions

Unlike liquid iron-light elements mixtures, the incorporation of heavy siderophile elements in liquid iron has not been studied much using first-principles computation. This study reports the computational results for four molten iron-rich alloys corresponding to 2.67 atom% of Ni, Co, Mo, and W at pressures up to 380 GPa and at temperatures 4000 to 7000 K using generalized gradient approximation. It is remarkable that a three-term form of the equation of state consisting of the reference pressure-volume isotherm $P(V,T_0)$, thermal pressure $B_{th}(T-T_0)$, and impurity pressure $B_{im}x$ accurately describes the calculated pressure-temperature-volume (P-V-T) results of all liquids. Moreover, the pressure is corrected for the apparent overestimation of liquid iron density relative to the recently reported high-pressure experimental data by adding the fourth term P_{emp} to the equation of state. The resulting density-pressure profile of pure iron liquid along a geotherm shows that the outer core suffers from a density deficient of ~ 6.8%, which is lower than most previous estimates by 1 to 2%. Our results show that the addition of Mo and W in liquid iron in any amount widens the density gap. Both Ni and Co do not affect the liquid density significantly and they almost behave as host iron atoms showing similar bond distances and local coordination. The mean lengths of Fe/Ni/Co-Fe bonds decrease from ~2.6 to ~2.15 Å and the mean Fe/Ni/Co-Fe coordination numbers increase from ~12.5 to ~13.5 over the entire pressure range considered. On the other hand, Mo and W show notable differences: The Mo/W-Fe bonds are longer than the Fe-Fe bonds by 5-6% and correspondingly, the mean iron coordination numbers of Mo/W atoms are higher than the mean Fe-Fe coordination numbers by 10-15%. All X-Fe and Fe-Fe coordination numbers thus exceed but remain close to 12. This means that the impurity atoms are incorporated via substitutional mechanism thus taking close-pack positions of iron atoms. In each alloy, impurity atoms are also found to be mostly non-interacting with each other and do not tend to form clusters. Based on these results, we suggest that each of these heavy elements is soluble in liquid iron in significant amount and may have facilitated core-mantle differentiation during the accretion phase. To constrain the amounts of these siderophile elements in the outer core requires more quantitative information about their behavior, including the diffusion rates and partitioning coefficients between silicate melts and metallic liquid.

Acknowledgements

The research was supported by NASA (80NSSC21K0377) and NSF (EAR 1463807). High computing resources were provided by Louisiana State University.

Appendix A. Supplementary material

Supplementary material related to this article is included.

References

Alfè, D., Kresse, G. and Gillan, M.J., 2000. Structure and dynamics of liquid iron under Earth's core conditions. Phys. Rev. B 61, 132-142.

Anderson, W.W., Ahrens, T.J., 1994. An equation of state for liquid iron and implications for the Earth's core. J. Geophys. Res. 99, 4273–4284.

Assael, M.J., Kakosimos, K., Banish, R.M., Brillo, J., Egry, I., Brooks, R., Quested, P.N., Mills, K.C., Nagashima, A., Sato, Y., and Wakeham, W.A., 2006. Reference data for the density and viscosity of liquid aluminum and liquid iron. J. Phys. Chem. Ref. Data 35, 285-300.

Badro, J., Coté, A.S., Brodholt, J.P., 2014. A seismologically consistent compositional model of Earth's core. Proc. Natl. Acad. Sci. 111, 7542–7545.

Bajgain, S.K., Mookherjee, M., and Dasgupta, R., 2021. Earth's core could be the largest terrestrial carbon reservoir. Comm. Earth Environ. 2, 165.

Brown, J.M., McQueen, R.G., 1986. Phase transitions, Grün isen parameter, and elasticity for shocked iron between 77 GPa and 400 GPa. J. Geophys. Res. 91, 7485–7494.

Dziewonski, A.M. and D.L. Anderson, 1981. Preliminary reference Earth model. Phys. Earth Planet. Inter. 25, 297-356.

Fei, Y. and Brosh, E., 2014. Experimental study and thermodynamic calculations of phase relations in the Fe–C system at high pressure. Earth Planet. Sci. Lett. 408, 155–162.

Fischer, R.A., Nakajima, Y., Campbell, A.J., Frost, D.J., Harries, D., Langenhorst, F., Miyajima, N., Pollok, K., Rubie, D.C., 2015. High pressure metal–silicate partitioning of Ni, Co, V, Cr, Si, and O. Geochim. Cosmochim. Acta 167, 177–194.

Hirose, K., Labrosse, S., Hernlund, J., 2013. Composition and state of the core. Annu. Rev. Earth Planet. Sci. 41, 657–691.

Huang, D., Siebert, J., and Badro J., 2021. High pressure partitioning behavior of Mo and W and late sulfur delivery during Earth's core formation. Geochim. Comochim. Acta 210, 19-31.

Ichikawa, H., Tsuchiya, T., Tange, Y., 2014. The P-V-T equation of state and thermodynamic properties of liquid iron. J. Geophys. Res., Solid Earth 119, 240–252.

Ichikawa, H. and Tsuchiya, T., 2020. Ab Initio thermoelasticity of liquid iron-nickel-light element alloys. Minerals 10, 59.

Karki, B.B., Ghosh, D.B., Maharjan, C., Karato, S-i, Park, J., 2018. Density-pressure profiles of Fe-bearing $MgSiO_3$ liquid: effects of valence and spin states, and implications for the chemical evolution of the lower mantle. Geophys. Res. Lett. 45, 3959–3966.

Kleine, T., Mün k r, C., Metzger, K., and Palme, H. (2002). Rapid accretion and early core formation on asteroids and the terrestrial planets from Hf- W chronometry. Nature 418, 952–955.

Kresse, G., Furthmü ller, J., 1996. Efficient iterative schemes for ab initio total-energy calculations using a plane-wave basis set. Phys. Rev. B54, 11169–11186.

Kuwayama, Y., Morard, G., Nakajima, Y., Hirose, K., Baron, A.Q.R., Kawaguchi, S.I., Tsuchiya, T., Ishikawa, D., Hirao, N., and Ohishi, Y., 2020. Equation of state of liquid iron under extreme conditions. Phys. Rev. Lett. 124, 165701.

McDonough, W.F. and Sun, S.s., 1995. The composition of the Earth. Chem. Geol. 120, 223-253.

Morard, G., Siebert, J., Andrault, D., Guignot, N., Garbarino, G., Guyot, F., Antonan-geli, D., 2013. The Earth's core composition from high pressure density measurements of liquid iron alloys. Earth Planet. Sci. Lett. 373, 169–178.

Perdew, J.P., Burke, K., Ernzerhof, M., 1996. Generalized gradient approximation made simple. Phys. Rev. Lett. 77, 3865–3868.

Poirier, J.P., 1994. Light elements in the Earths outer core: a critical review. Phys. Earth Planet. Inter. 85, 319–337.

Posner, E.S. and Steinle-Neumann, G., 2019. Mass transport and structural properties of binary liquid iron alloys at high pressure. Geochem. Geophys. Geosys. 20, 3556-3568.

Rubie, D.C., Melosh, H. J., Reid, J. E., Liebske, C. and Righter, K., 2003. Mechanisms of metal–silicate equilibration in the terrestrial magma ocean. Earth Planet. Sci. Lett. 205, 239-255.

Sakamaki, K., Takahashi, E., Nakajima, Y., Nishihara, Y., Funakoshi, K., Suzuki, T., Fukai, Y., 2009. Melting phase relation of FeH_x up to 20 GPa: implication for the temperature of the Earth's core. Phys. Earth Planet. Inter. 174, 192–201.

Tagawa, S., Sakamoto, N., Hirose, K., Yokoo, S., Hernlund, J., Ohishi, Y., Yurimoto, H., 2021. Experimental evidence for hydrogen incorporation into Earth's core. Nature Comm. 12, 2588.

Samuel, H., 2012. A re- evaluation of metal diapir breakup and equilibration in terrestrial magma oceans. Earth Planet. Sci. Lett. 313, 105–114.

Umemoto, K., Hirose, K., 2015. Liquid iron-hydrogen alloys at outer core conditions by first-principles calculations. Geophys. Res. Lett. 42, 7513–7520.

Umemoto, K. and Hirose, K., 2020. Chemical compositions of the outer core examined by first principles calculations. Earth Planet. Sci. Lett. 531, 116009.

Wagle, F., Steinle-Neumann, G., 2019. Liquid iron equation of state to the terapascal regime from ab initio simulations. J. Geophys. Res. 124, 3350–3364.

Wood, B.J., Walter, M.J., and Wade, J., 2006. Accretion of the Earth and segregation of its core. Nature 441, 825-833.

Zou, Z., Koper, K.D., Cormier, V. F., 2008. The structure of the base of the outer core inferred from seismic waves diffracted around the inner core. J. Gephys. Res. 113, B05314.

Figure Captions and Figures

Fig. 1. Calculated pressure-volume-temperature results (symbols) and the equation of state isotherms (curves) of pure liquid iron.

Fig. 2. **A**) Thermal pressure (P_{th}) defined relative to 5000 K for pure iron (open circles) and all four binary alloys (filled circles) as a function of compression. The model results are shown by lines. **B**) Impurity-induced pressure (P_{im}) defined relative to pure iron for four liquid alloys (different symbols as shown) as a function of compression. The model results shown by curves.

Fig. 3. Calculated pressure-volume-temperature results (symbols) and the equation of state isotherms (curves) of four binary alloy liquids: $Fe_{146}Ni_4$, $Fe_{146}Co_4$, $Fe_{146}Mo_4$, and $Fe_{146}W_4$.

Fig. 4. Specific heat capacity (**A**) and thermal Grüneisen parameter (**B**) calculated as constant values in the temperature range 4000 to 7000 K of pure iron and four alloy liquids as shown in the legend. The calculated results of pure iron liquid are also shown at 2500 K (gray filled circles) and 3500 K (open circles).

Fig. 5. Fe-Fe radial distribution function (RDF, in arbitrary units) for pure liquid iron and four X-Fe partial RDFs corresponding to Ni and Co-bearing (**A**) and Mo- and W-bearing (**B**) liquids at two temperature-volume conditions.

Fig. 6. Mean X-Fe bond distances for four liquid alloys with X = Ni, Co, Mo, and W (different symbols) in comparison with the pure iron Fe-Fe results (curves). In each case, the different pressure intervals are covered at different temperatures: 2000 K (gray curve), 3000 K (cyan curve), 4000 K (blue curve/symbols), 5000 K (black curve/symbols), 6000 K (red curve/symbols), and 7000 K (green curve/symbols).

Fig. 7. A) Mean Fe-Fe coordination number (Z_{FeFe}) for pure iron (curves) and four liquid alloys shown by different symbols. **B**) Mean X-Fe coordination number (Z_{XFe}) for four alloys with X = Ni, Co, Mo, and W (different symbols) in comparison with the pure iron number (curves). In each case, the different pressure intervals are covered at different temperatures, 2000 K (gray curve), 3000 K (cyan curve), 4000 K (blue curve/symbols), 5000 K (black curve/symbols), 6000 K (red curve/symbols), and 7000 K (green curve/symbols).

Fig. 8. Corrected density-pressure profiles of liquid iron at temperatures from 2000 to 7000 K (solid curves from left to right) compared with the measured data at 0 GPa and 1811 K (Assael et al., 2006) and elevated pressures up to 116 GPa at temperatures 2600 to 4350 K (Kuwayama et al., 2020), and shock-wave data at high pressures (Anderson and Ahrens, 1994). The pressure is corrected by adding empirical term P_{emp} shown in the inset (straight line) which describes the difference in pressure between the computations and experiments as a function of compression. The density profile of pure liquid iron along the isentrope (4293 to 5800 K) across the outer core is compared with the seismic data (PREM).

Fig. 9. Calculated densities of four iron-rich alloy liquids ($Fe_{146}Ni_4$, $Fe_{146}Co_4$, $Fe_{146}Mo_4$, and $Fe_{146}W_4$) compared with pure liquid iron density (solid curve) at 5000 K and seismic density profile (PREM) over the entire core regime. The results of Ni- and Co-bearing liquids are shown by symbols at a few pressures for the sake of clarity. The pressure is calculated using the three-term form of the equation of state (Eq. 3) with inclusion of the empirical correction (Eq. 5).

Fig. 1

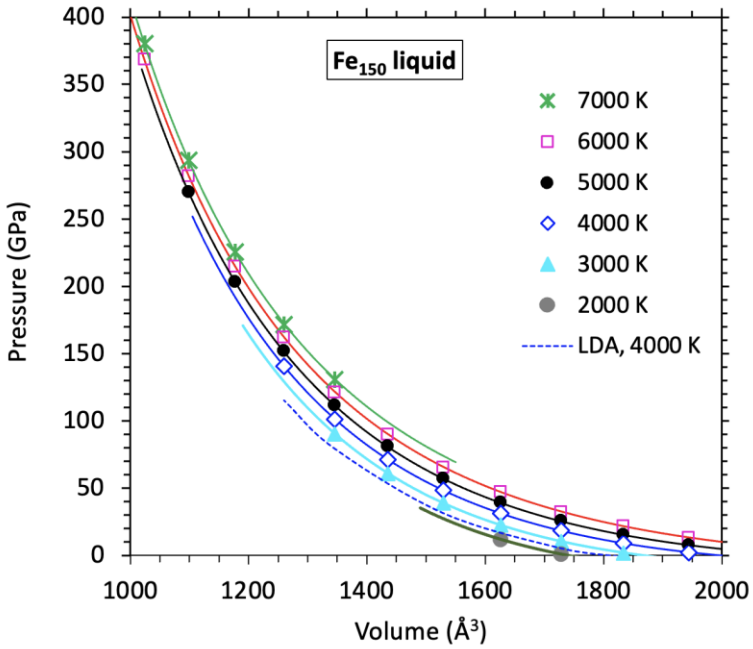
Fe150 liquid
7000 K
6000 K
5000 K
4000 K
3000 K
2000 K
LDA, 4000 K
Pressure (GPa)
Volume (Å3)
400
350
300
250
200
150
100
50
0
1000
1200
1400
1600
1800
2000

Fig. 2

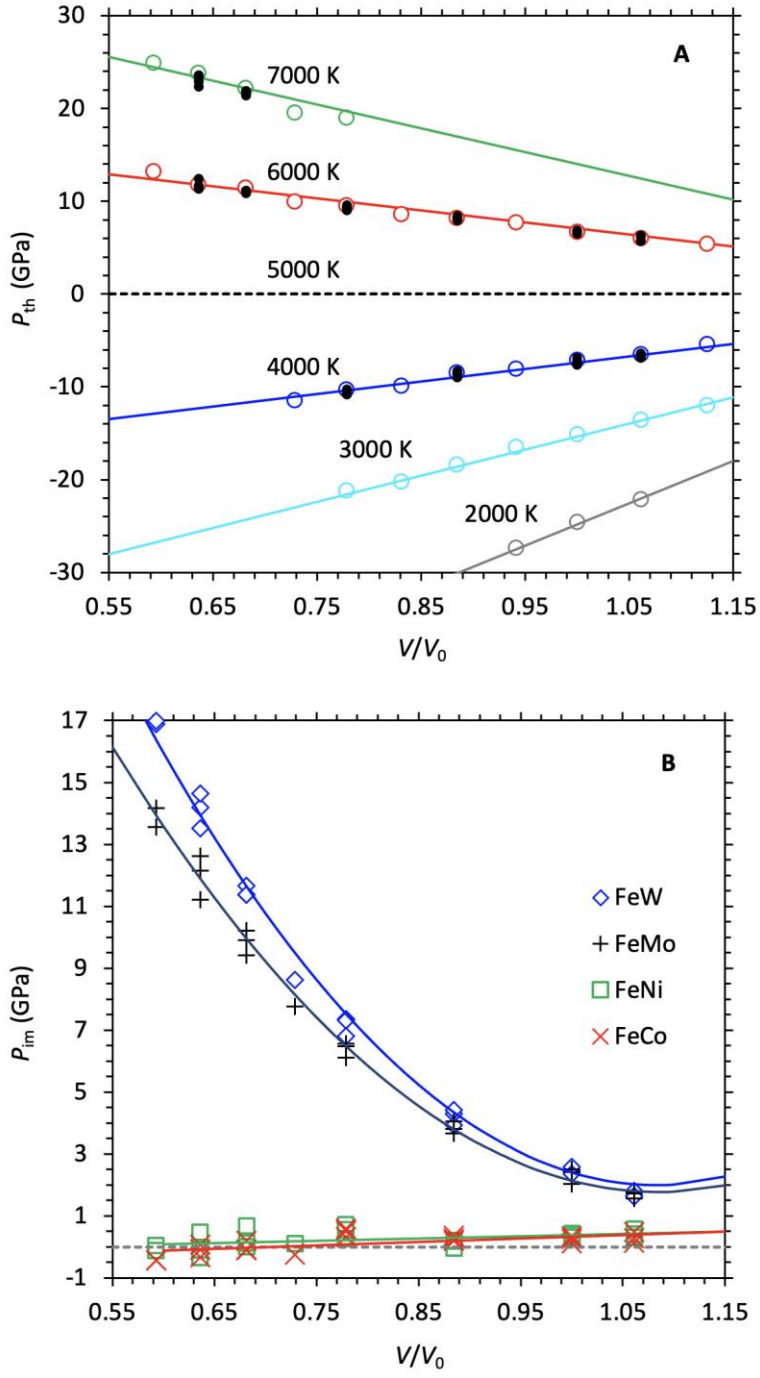
A
7000 K
6000 K
5000 K
4000 K
3000 K
2000 K
P_{th} (GPa)
V/V_0
B
FeW
FeMo
FeNi
FeCo
P_{im} (GPa)
V/V_0

Fig. 3

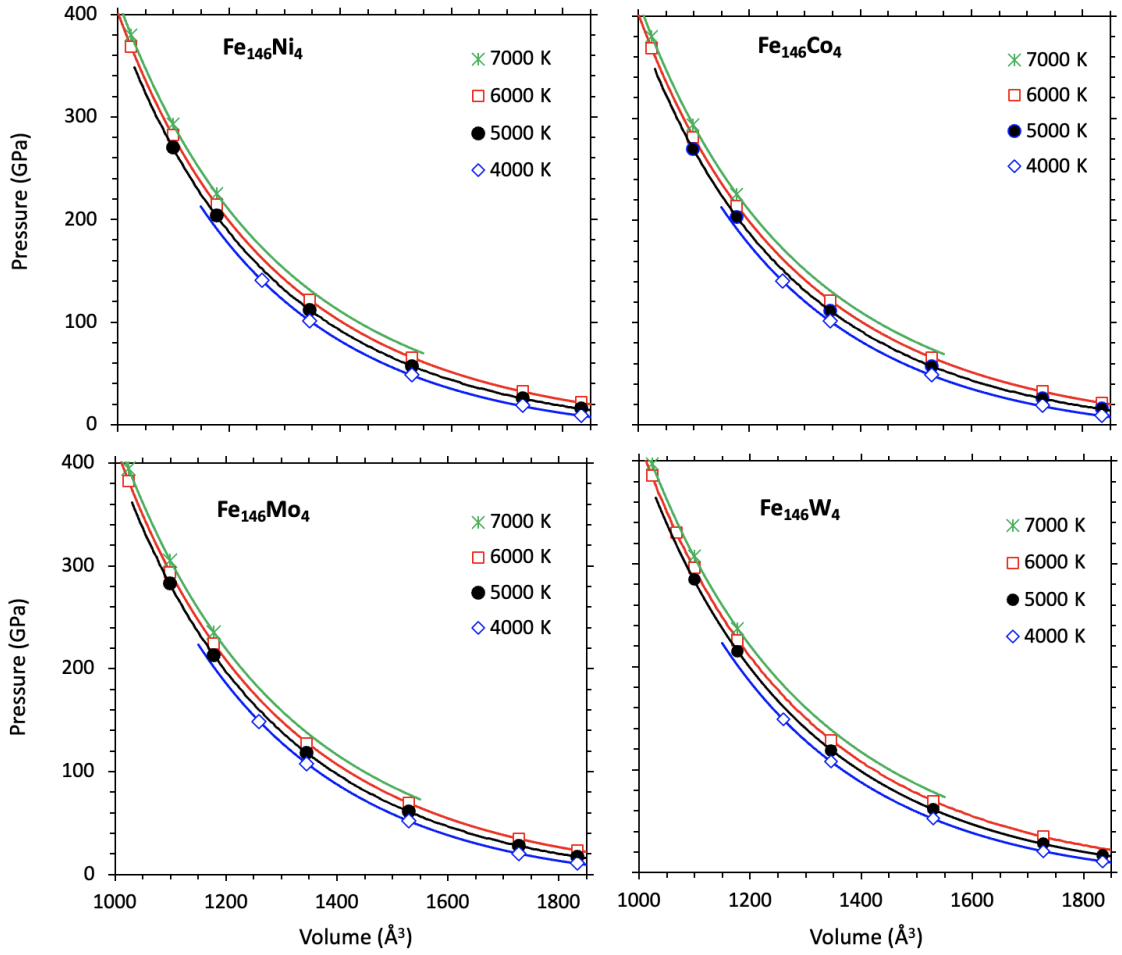
Fe146Ni4
Fe146Co4
Fe146Mo4
Fe146W4
7000 K
6000 K
5000 K
4000 K
Pressure (GPa)
Volume (Å3)
0
100
200
300
400
1000
1200
1400
1600
1800

Fig. 4

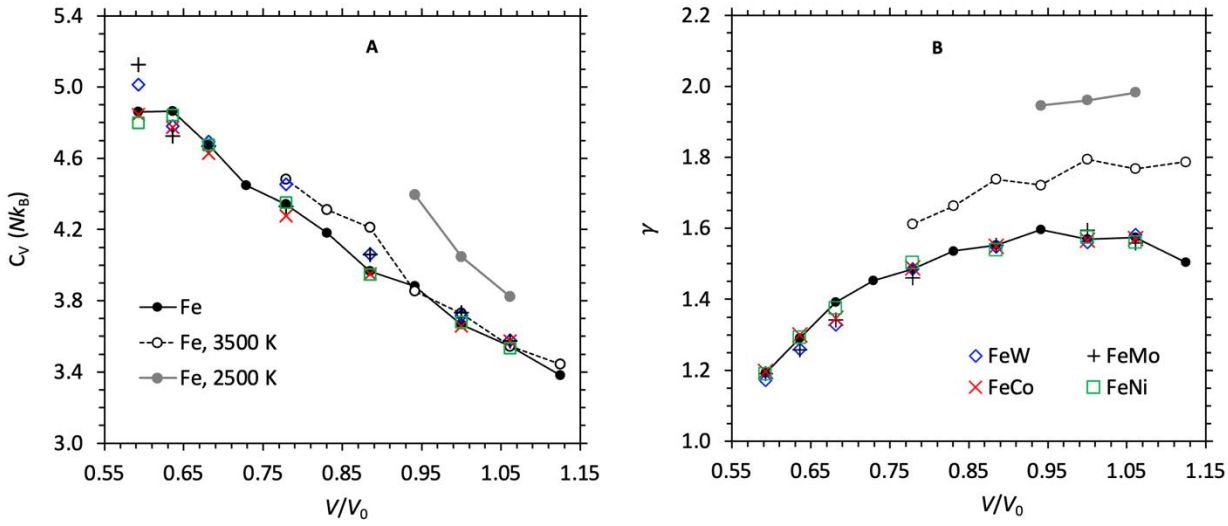
A
B
C_V (Nk_B)
γ
V/V_0
Fe
Fe, 3500 K
Fe, 2500 K
FeW
FeMo
FeCo
FeNi

Fig. 5

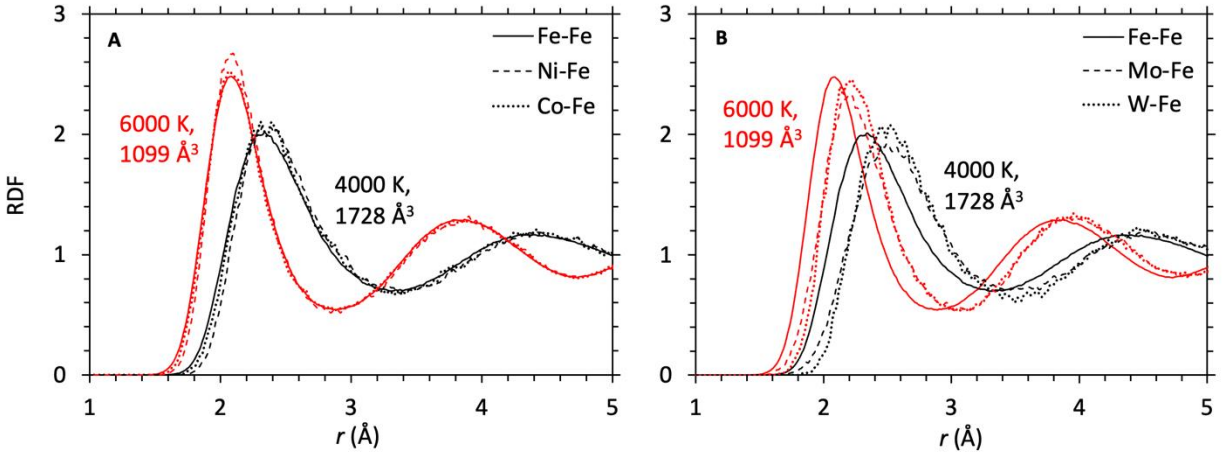
A
B
RDF
r (Å)
Fe-Fe
Ni-Fe
Co-Fe
Mo-Fe
W-Fe
6000 K,
1099 Å^3
4000 K,
1728 Å^3

Fig. 6

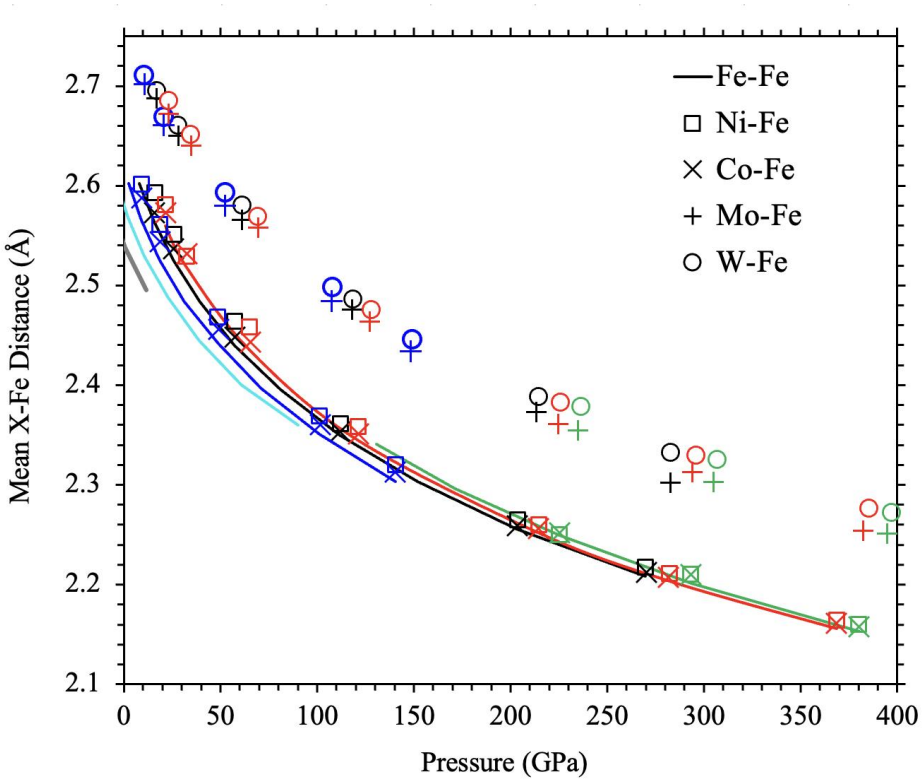
Fe-Fe
Ni-Fe
Co-Fe
Mo-Fe
W-Fe
Mean X-Fe Distance (Å)
Pressure (GPa)
2.7
2.6
2.5
2.4
2.3
2.2
2.1
0
50
100
150
200
250
300
350
400

Fig. 7

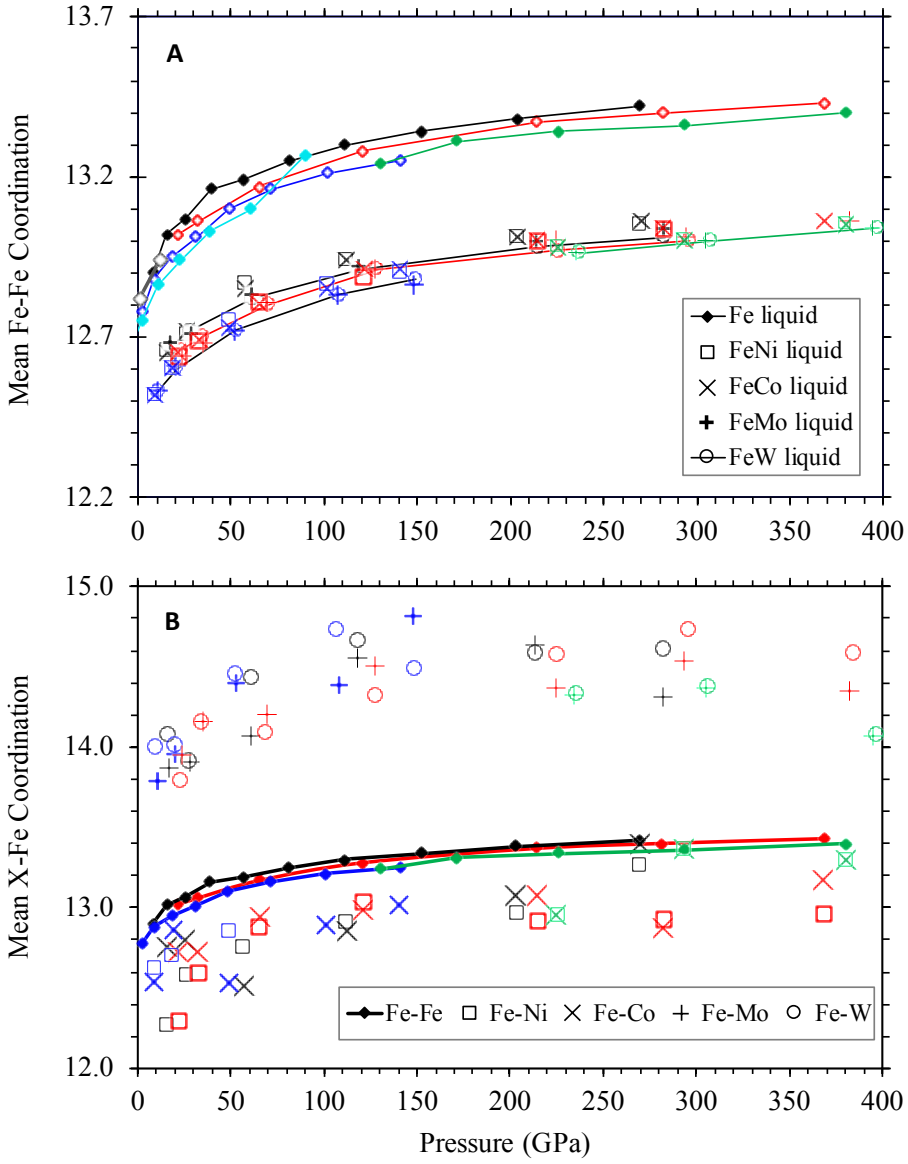
A
B
Mean Fe-Fe Coordination
Mean X-Fe Coordination
Pressure (GPa)
Fe liquid
FeNi liquid
FeCo liquid
FeMo liquid
FeW liquid
Fe-Fe
Fe-Ni
Fe-Co
Fe-Mo
Fe-W
13.7
13.2
12.7
12.2
15.0
14.0
13.0
12.0
0
50
100
150
200
250
300
350
400

Fig. 8

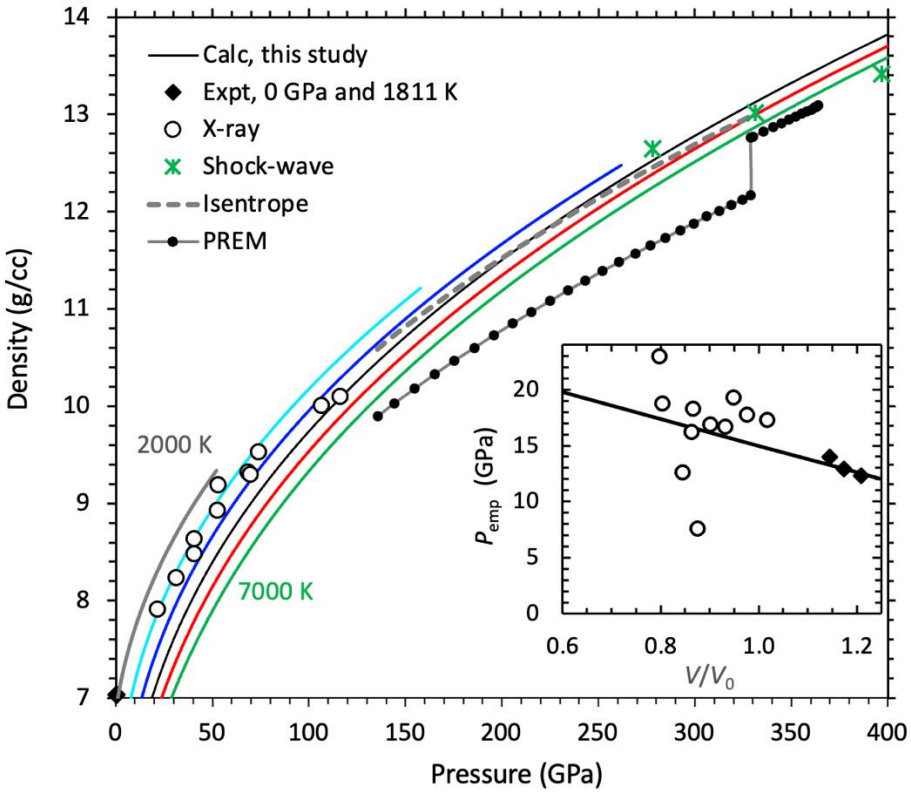
Calc, this study
Expt, 0 GPa and 1811 K
X-ray
Shock-wave
Isentrope
PREM
2000 K
7000 K
Density (g/cc)
Pressure (GPa)
P_{emp} (GPa)
V/V_0

Fig. 9

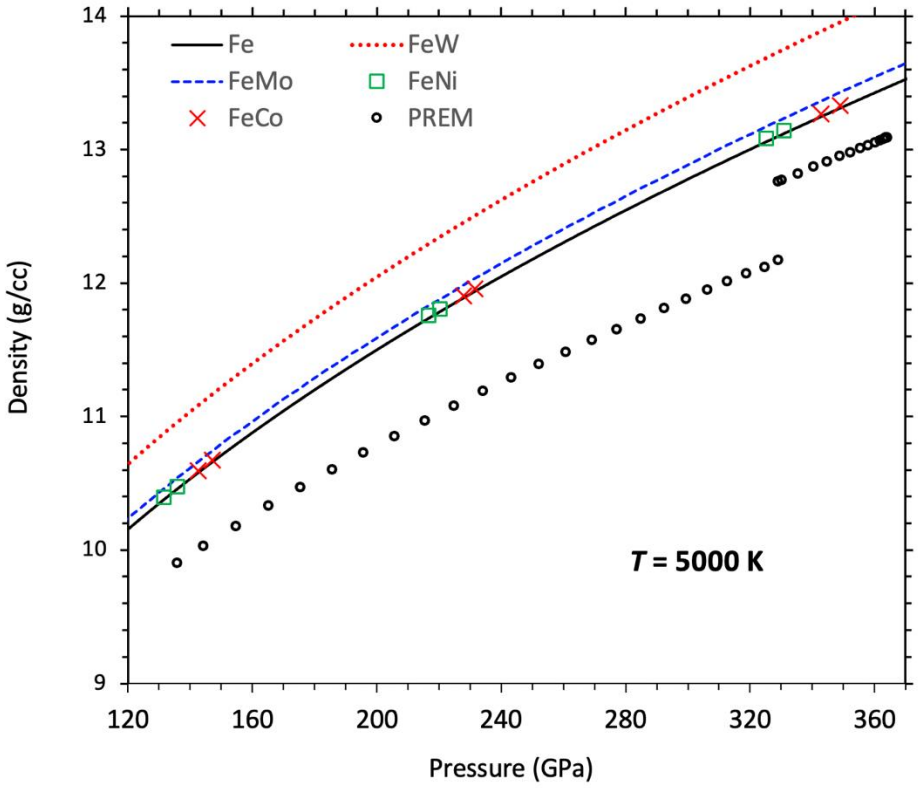
Fe
FeW
FeMo
FeNi
FeCo
PREM
T = 5000 K
Density (g/cc)
Pressure (GPa)
14
13
12
11
10
9
120
160
200
240
280
320
360

Highlights

First-principles simulations of iron-rich liquids containing heavy siderophile elements (Ni, Co, Mo, and W) at high pressures and temperatures

Calculated local structures suggest substitutional incorporation and no clustering activity of impurity elements

Mo and W dissolved in liquid iron behave differently than Ni and Co and widen the apparent density gap between iron-rich liquid and outer core

Graphical Abstract:

Not Applicable

Figure Captions and Figures

Fig. 1. Calculated pressure-volume-temperature results (symbols) and the equation of state isotherms (curves) of pure liquid iron.

Fig. 2. **A**) Thermal pressure (P_{th}) defined relative to 5000 K for pure iron (open circles) and all four binary alloys (filled circles) as a function of compression. The model results are shown by lines. **B**) Impurity-induced pressure (P_{im}) defined relative to pure iron for four liquid alloys (different symbols as shown) as a function of compression. The model results shown by curves.

Fig. 3. Calculated pressure-volume-temperature results (symbols) and the equation of state isotherms (curves) of four binary alloy liquids: $Fe_{146}Ni_4$, $Fe_{146}Co_4$, $Fe_{146}Mo_4$, and $Fe_{146}W_4$.

Fig. 4. Specific heat capacity (**A**) and thermal Grüneisen parameter (**B**) calculated as constant values in the temperature range 4000 to 7000 K of pure iron and four alloy liquids as shown in the legend. The calculated results of pure iron liquid are also shown at 2500 K (gray filled circles) and 3500 K (open circles).

Fig. 5. Fe-Fe radial distribution function (RDF, in arbitrary units) for pure liquid iron and four X-Fe partial RDFs corresponding to Ni and Co-bearing (**A**) and Mo- and W-bearing (**B**) liquids at two temperature-volume conditions.

Fig. 6. Mean X-Fe bond distances for four liquid alloys with X = Ni, Co, Mo, and W (different symbols) in comparison with the pure iron Fe-Fe results (curves). In each case, the different pressure intervals are covered at different temperatures: 2000 K (gray curve), 3000 K (cyan curve), 4000 K (blue curve/symbols), 5000 K (black curve/symbols), 6000 K (red curve/symbols), and 7000 K (green curve/symbols).

Fig. 7. A) Mean Fe-Fe coordination number (Z_{FeFe}) for pure iron (curves) and four liquid alloys shown by different symbols. **B**) Mean X-Fe coordination number (Z_{XFe}) for four alloys with X = Ni, Co, Mo, and W (different symbols) in comparison with the pure iron number (curves). In each case, the different pressure intervals are covered at different temperatures, 2000 K (gray curve), 3000 K (cyan curve), 4000 K (blue curve/symbols), 5000 K (black curve/symbols), 6000 K (red curve/symbols), and 7000 K (green curve/symbols).

Fig. 8. Corrected density-pressure profiles of liquid iron at temperatures from 2000 to 7000 K (solid curves from left to right) compared with the measured data at 0 GPa and 1811 K (Assael et al., 2006) and elevated pressures up to 116 GPa at temperatures 2600 to 4350 K (Kuwayama et al., 2020), and shock-wave data at high pressures (Anderson and Ahrens, 1994). The pressure is corrected by adding empirical term P_{emp} shown in the inset (straight line) which describes the difference in pressure between the computations and experiments as a function of compression.

The density profile of pure liquid iron along the isentrope (4293 to 5800 K) across the outer core is compared with the seismic data (PREM).

Fig. 9. Calculated densities of four iron-rich alloy liquids ($Fe_{146}Ni_4$, $Fe_{146}Co_4$, $Fe_{146}Mo_4$, and $Fe_{146}W_4$) compared with pure liquid iron density (solid curve) at 5000 K and seismic density profile (PREM) over the entire core regime. The results of Ni- and Co-bearing liquids are shown by symbols at a few pressures for the sake of clarity. The pressure is calculated using the three-term form of the equation of state (Eq. 3) with inclusion of the empirical correction (Eq. 5).

Fig. 1

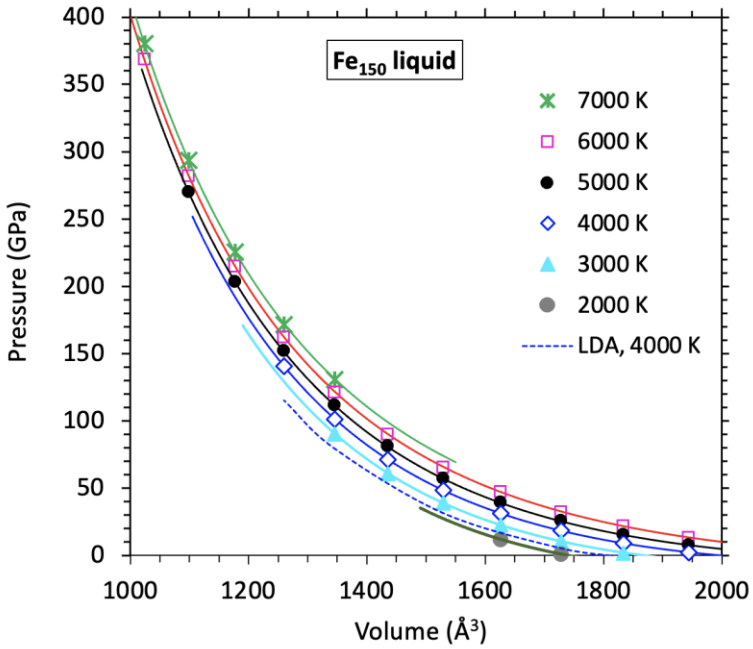
Fe150 liquid
7000 K
6000 K
5000 K
4000 K
3000 K
2000 K
LDA, 4000 K
Pressure (GPa)
Volume (Å3)
400
350
300
250
200
150
100
50
0
1000
1200
1400
1600
1800
2000

Fig. 2

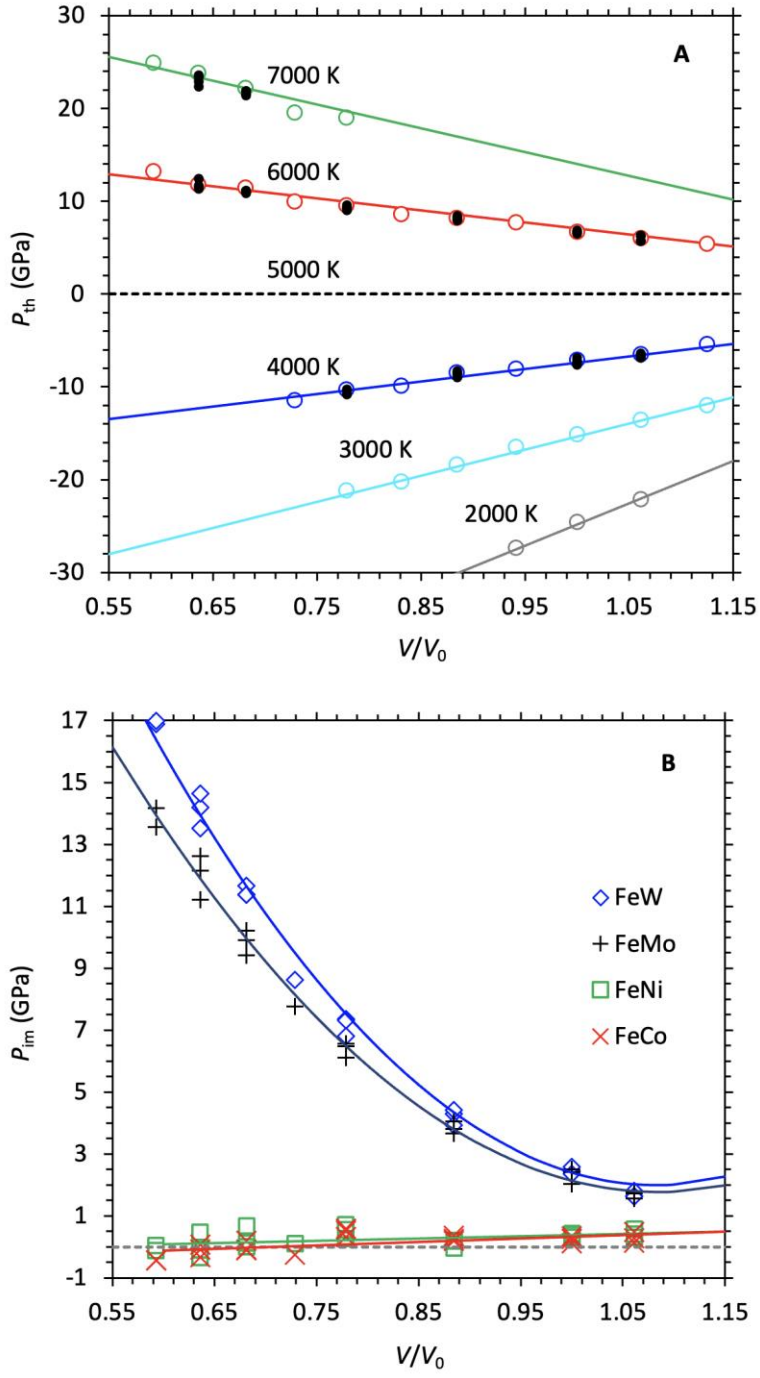
A
7000 K
6000 K
5000 K
4000 K
3000 K
2000 K
P_{th} (GPa)
V/V_0
B
FeW
FeMo
FeNi
FeCo
P_{im} (GPa)
V/V_0

Fig. 3

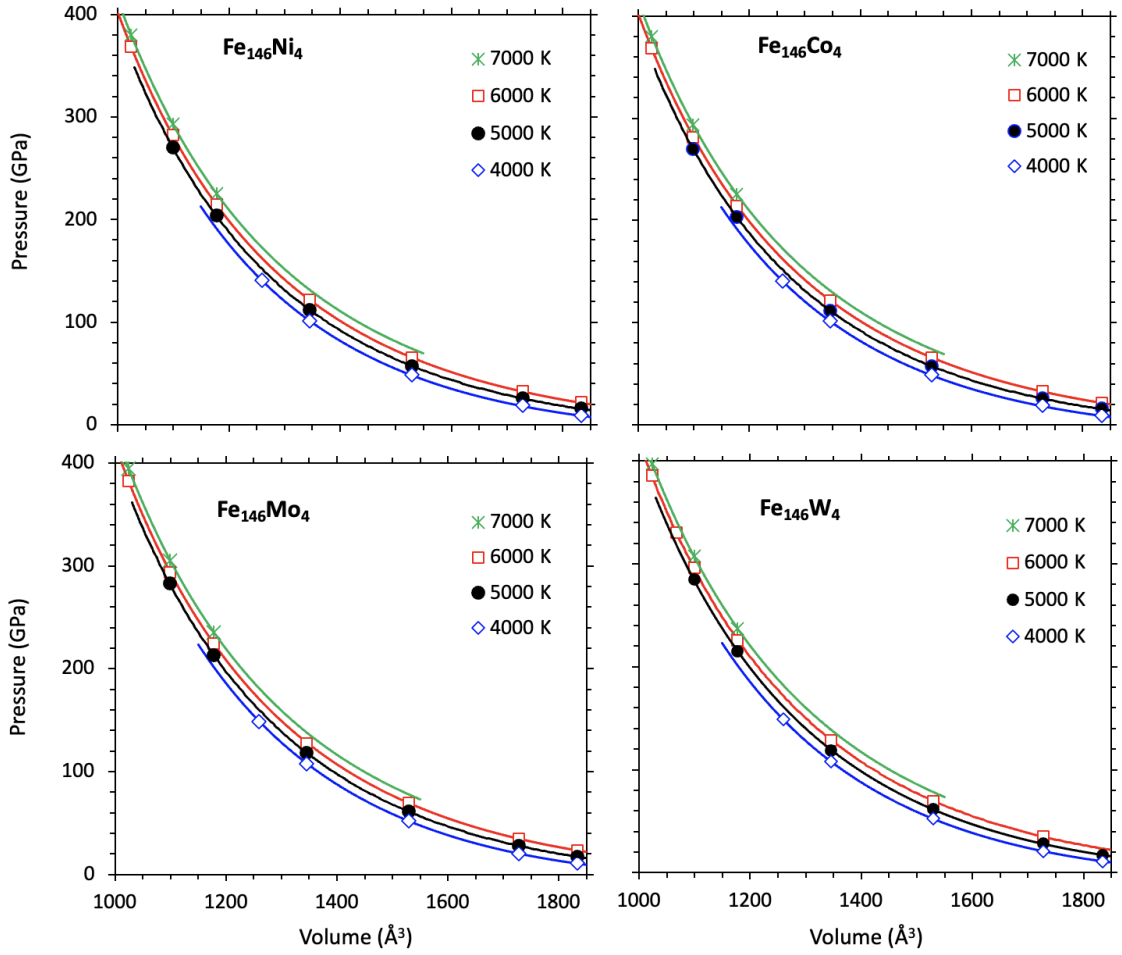
Fe146Ni4
Fe146Co4
Fe146Mo4
Fe146W4
7000 K
6000 K
5000 K
4000 K
Pressure (GPa)
Volume (Å3)
0
100
200
300
400
1000
1200
1400
1600
1800

Fig. 4

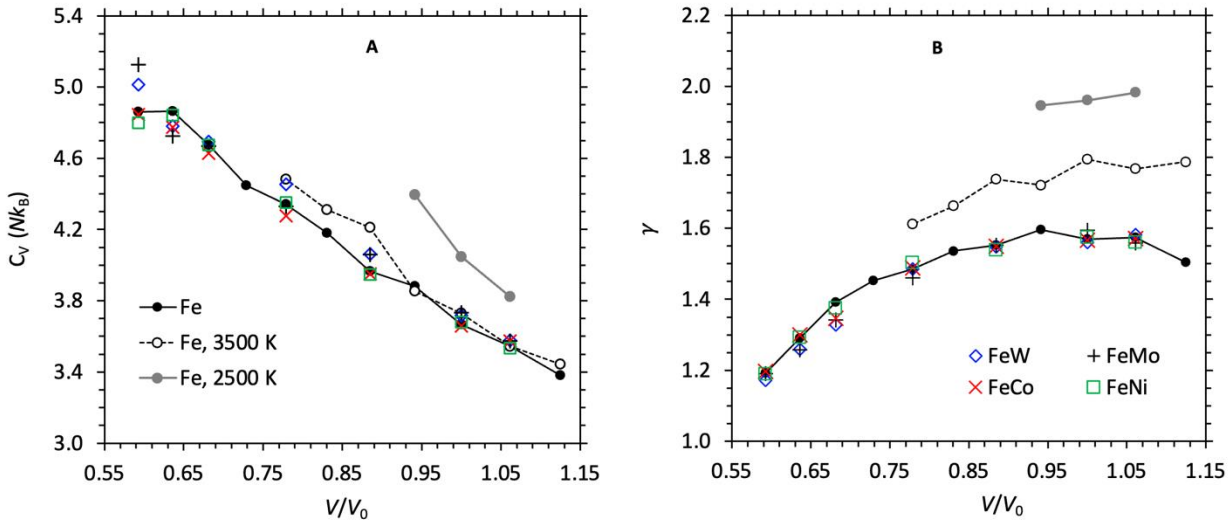
A
B
C_V (Nk_B)
γ
V/V_0
Fe
Fe, 3500 K
Fe, 2500 K
FeW
FeMo
FeCo
FeNi

Fig. 5

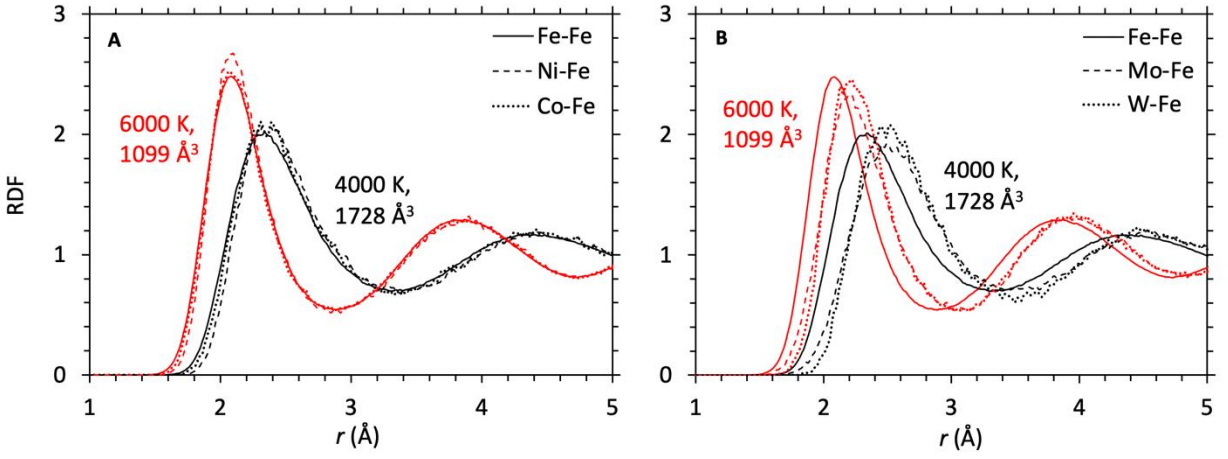
A
B
RDF
r (Å)
Fe-Fe
Ni-Fe
Co-Fe
Mo-Fe
W-Fe
6000 K,
1099 Å^3
4000 K,
1728 Å^3

Fig. 6

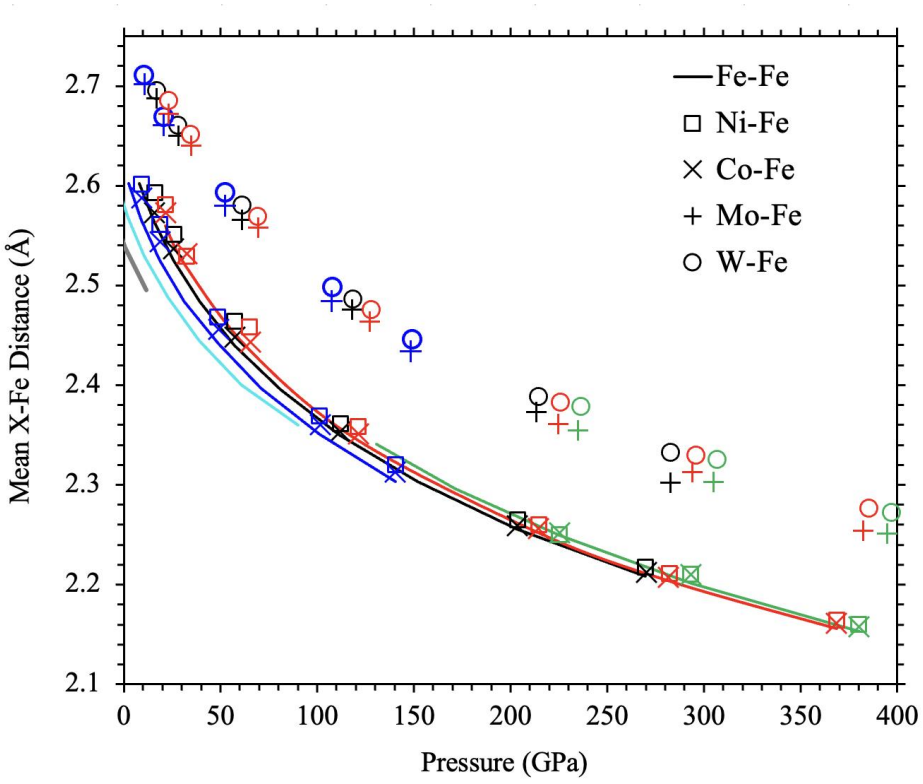
Fe-Fe
Ni-Fe
Co-Fe
Mo-Fe
W-Fe
Mean X-Fe Distance (Å)
Pressure (GPa)
2.7
2.6
2.5
2.4
2.3
2.2
2.1
0
50
100
150
200
250
300
350
400

Fig. 7

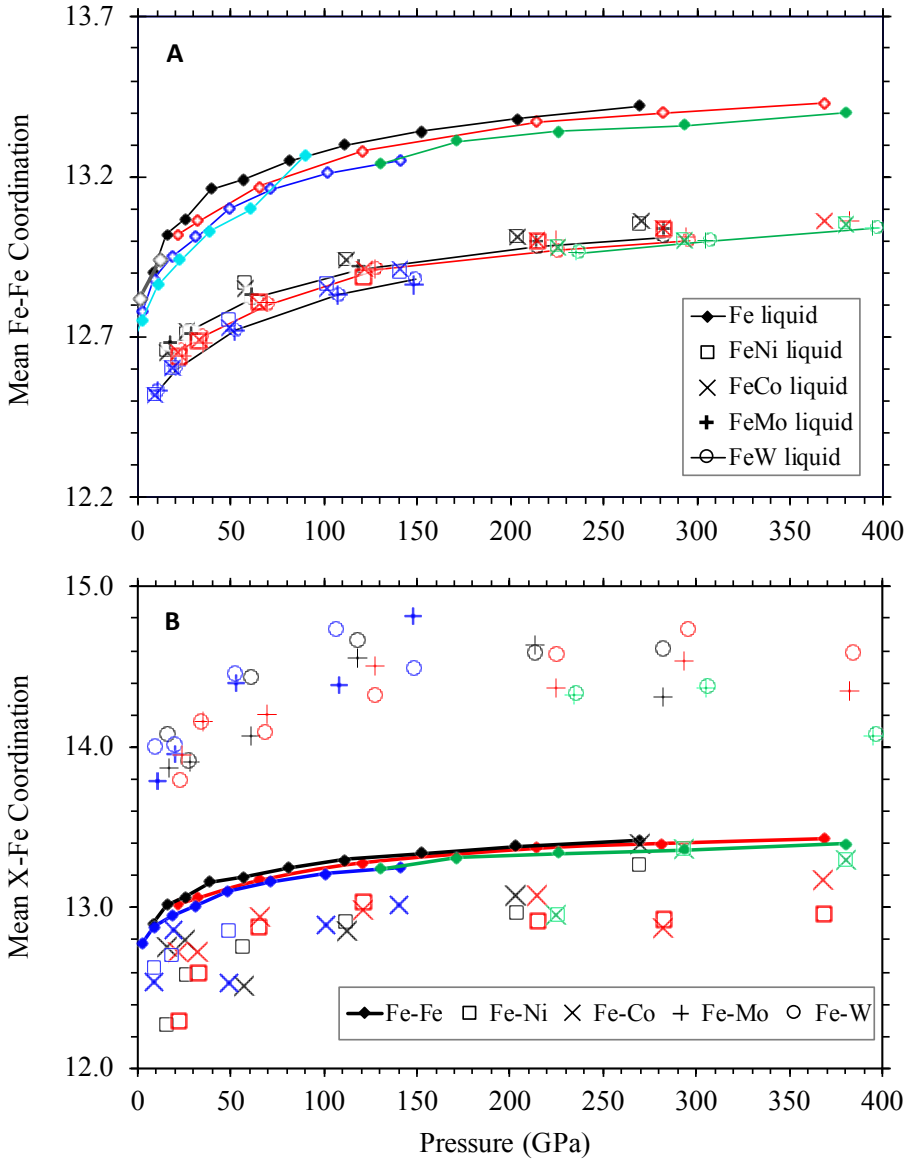
A
B
Mean Fe-Fe Coordination
Mean X-Fe Coordination
Pressure (GPa)
Fe liquid
FeNi liquid
FeCo liquid
FeMo liquid
FeW liquid
Fe-Fe
Fe-Ni
Fe-Co
Fe-Mo
Fe-W
13.7
13.2
12.7
12.2
15.0
14.0
13.0
12.0
0
50
100
150
200
250
300
350
400

Fig. 8

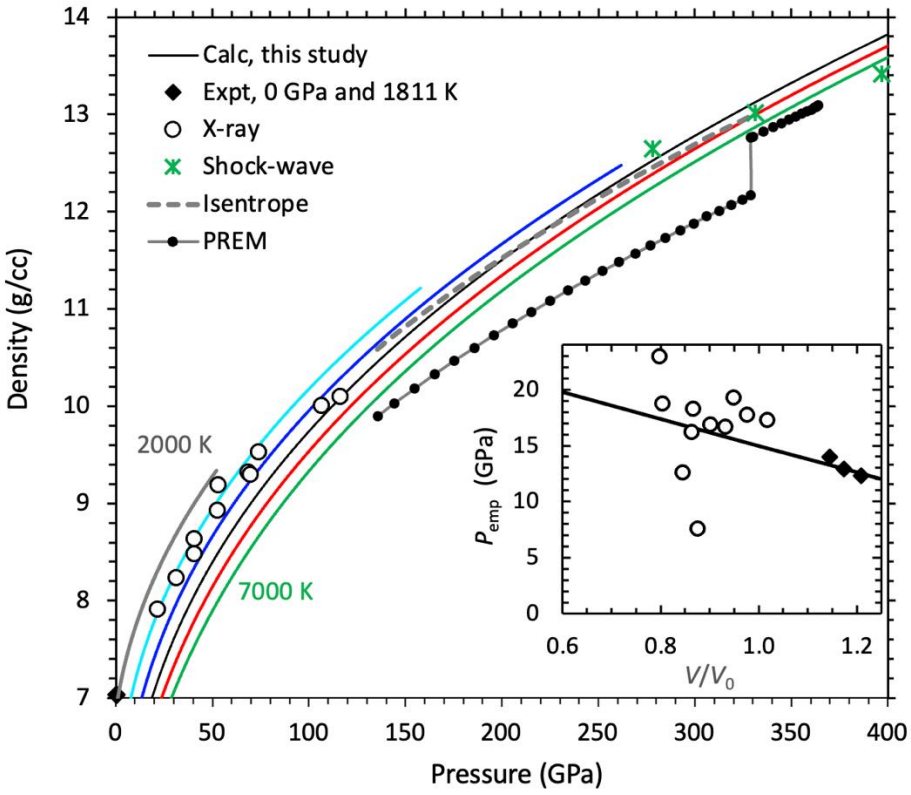
Calc, this study
Expt, 0 GPa and 1811 K
X-ray
Shock-wave
Isentrope
PREM
2000 K
7000 K
Density (g/cc)
Pressure (GPa)
P_{emp} (GPa)
V/V_0

Fig. 9

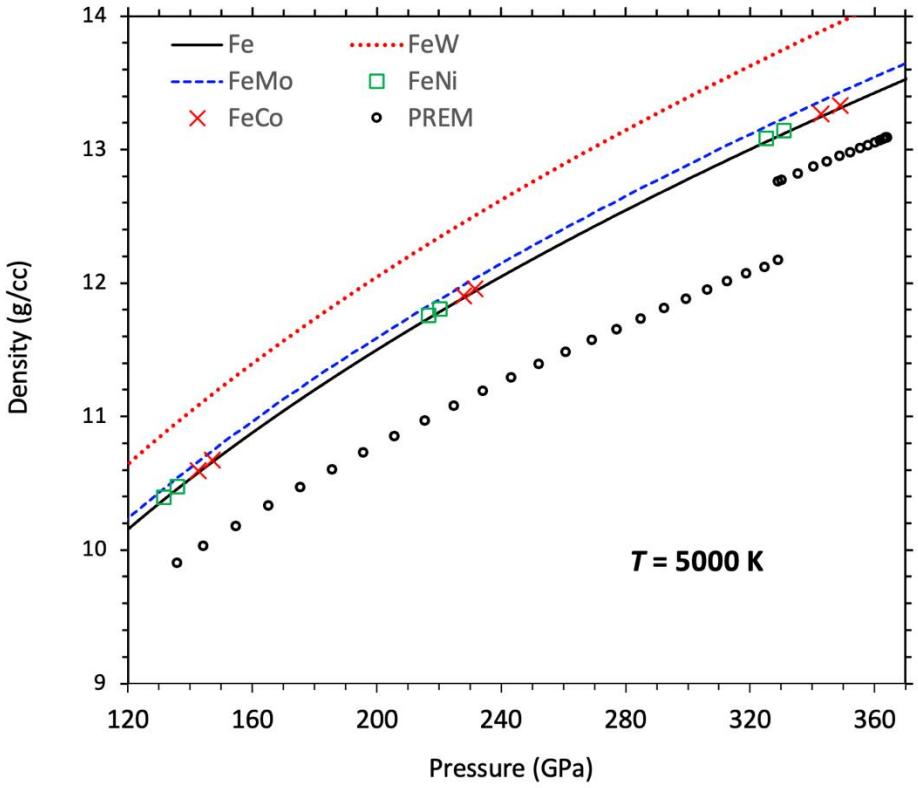
Fe
FeW
FeMo
FeNi
FeCo
PREM
T = 5000 K
Density (g/cc)
Pressure (GPa)
14
13
12
11
10
9
120
160
200
240
280
320
360

Declaration of interests

☒The authors declare that they have no known competing financial interests or personal relationships that could have appeared to influence the work reported in this paper.

☐The authors declare the following financial interests/personal relationships which may be considered as potential competing interests:

B.B.K. designed research and D.B. performed simulations. All authors contributed to the analysis and discussion of the results, and to the preparation of the manuscript.

First-principles simulations of liquid iron-heavy element alloys at high pressure

Dipendra Banjara[a], Dipta B Ghosh[a,b] and Bijaya B Karki[a,b,c,*]

[a]*School of Electrical Engineering and Computer Science*, [b]*Department of Geology and Geophysics*, [c]*Center for Computation and Technology, Louisiana State University, Baton Rouge, LA 70803, USA*

[*]Corresponding author: bbkarki@lsu.edu (B.B. Karki)

ABSTRACT

Iron-rich metallic liquid in the Earth's outer core is thought to contain many elements. While the incorporation of light elements in liquid iron has been widely studied, liquid iron-heavy element mixtures, particularly considering Co, Mo, and W which are relevant in constraining core-forming conditions need more studies. Here we investigate the thermodynamic and structural behavior of these siderophile elements and Ni dissolved in liquid iron in the amount of 2.67 atom% using first-principles molecular dynamics over the pressure range of the entire Earth's interior at temperatures 4000 to 7000 K. The calculated pressure-volume-temperature results of these iron-rich alloys are accurately described by adding the appropriative terms to the equation of state of pure iron liquid to account for the effects of temperature and impurity. The calculated mean iron coordination number of Mo and W is somewhat larger than that of Ni and Co and host iron atoms thus implying substitutional incorporation mechanism. The lack of clustering activity among the impurity atoms means that each of these impurity elements is soluble in liquid iron. Our analysis also shows that Mo and W increase the liquid density much more than Ni and Co mainly for mass reason while the bulk modulus remains essentially unaffected in all cases. The presence of heavy elements widens the apparent density gap between iron-rich liquid and the outer core so additional amounts of lighter impurity elements should be considered when constraining the core composition.

1. Introduction

Iron is considered as the main constituent of the Earth's core. Molten iron shows large density (8 - 10%) and velocity (4-5%) differences with respect to the outer liquid core (e.g., Anderson and Ahrens, 1994; Alfe et al., 2000; Ichikawa et al., 2014; Kuwayama et al., 2020). Therefore, light elements, such as H, C, N, O, S, etc. must be incorporated in liquid iron to explain the discrepancy (e.g., Poirier, 1995; Morard et al., 2013; Badro et al., 2014; Tagawa et al., 2021). Any volatile impurities not only lower the density of liquid iron-rich alloy but also raise its bulk sound velocity to make these properties comparable to the seismic profiles of the outer core. They also lower the melting temperature of iron and thus help the outer core remain in the liquid state (Sakamaki et al. 2008; Fei and Brosh, 2014)). Under inner core conditions, the light elements are also incorporated in solid iron though in lesser amounts because of smaller density deficit.

Based on geochemical, cosmological, and meteoritical arguments, the composition of the outer core perhaps is even more complex (McDonough and Sun, 1995; Hirose et al., 2013). During the core formation by accretion of planetary embryos and impacting planetesimals, siderophile elements could have disproportionately partitioned into the metallic core while lithophile elements were left behind in the silicate mantle. For instance, refractory siderophile elements, including Ni, Co, Mo, and W may have been swept down into the core with molten iron in significant amounts. Nickel is present in liquid iron in several percent (~5%) while Co, Mo, and W are present in much smaller amounts (less than 1% together). Despite their small amounts, Co, Mo, and W are considered to serve as important tracers for the conditions and timing of core formation (e.g., Rubie et al., 2003; Fischer et al., 2015; Huang et al., 2021). How these geochemically significant elements behave in liquid iron and how they influence host properties help us better understand the formation and evolution of the core.

Iron-rich liquids have been studied extensively under varying conditions of pressure and temperature using both computational and experimental methods. First-principles computational approach has so far focused on pure iron liquid (Alfe et al., 2000; Ichikawa et al., 2014) and iron-light element mixtures (Badro et al., 2014; Umemoto and Hirose, 2015; Ichikawa and Tsuchiya, 2020; Bajgain et al., 2021) with the aim of constraining the concentration of each alloying element that can match the seismic density and velocity profiles of the outer core. These computations have investigated the equation of state, structure, and diffusivity of binary iron-rich and some Fe-Ni ternary systems. Such studies are not yet done in the context of liquid iron-heavy element mixtures considering Co, Mo, and W. On the other hand, experiments have investigated a wide range of properties, including density and metal-silicate partitioning, but they are generally confined to relatively narrow pressure and temperature conditions (Fisher et al., 2015; Huang et al., 2021; Tagawa et al., 2021). A recent experimental study of pure liquid iron has reported the density up to 116 GPa and 4350 K by diffuse x-ray scattering and the bulk sound velocity up to 46 GPa and 2700 K by inelastic x-ray scattering (Kuwayama et al., 2020). These data complement the shock-

wave data at 278-397 GPa (Brown and McQueen, 1986; Anderson and Ahrens, 1994). Thus, the density data are still not available at almost all conditions of the outer core.

Here we report a first-principles study of four iron-rich liquid alloys considering heavy elements, including Ni, Co, Mo, and W. While FeNi liquid was previously simulated (Posner and Steinle-Neumann, 2019; Umemoto and Hirose, 2020; Ichikawa and Tsuchiya, 2020), the computational study of Co, Mo, and W-bearing iron alloy liquids is still lacking. Our focus is on the equation of state and structural behavior of these four alloys in comparison to the pure iron liquid at pressures up to 380 GPa and temperatures up to 7000 K thus covering the pressure-temperature conditions of the entire earth's interior. We also present implications of our structural and density results for the outer core and core formation.

2. Methods

First-principles molecular dynamics (FPMD) simulations were performed within the generalized gradient approximation (GGA) and projector augmented wave formalism using VASP - Vienna ab initio simulation package (Kresse and Furthmüller, 1996). The GGA functional used was Perdew-Burke-Ernzerhof type as in most previous computational studies (Perdew et al., 1996). The gamma point was used for Brillouin zone sampling and the energy cutoff of 400 eV was used for plane wave basis set.

The simulation supercell consisted of 150 atoms for pure iron liquid (Fe_{150}). To simulate each FeX system where X = Ni, Co, Mo, and W, four randomly selected iron atoms in the liquid iron supercell were replaced with the respective alloying element. We thus generated four independent supercells with compositions $Fe_{146}Ni_4$, $Fe_{146}Co_4$, $Fe_{146}Mo_4$, and $Fe_{146}W_4$, each of which corresponds to an impurity concentration of 2.67 atom%. In the case of W-bearing alloy, we also considered a higher concentration of 5.33 atom% by using $Fe_{142}W_8$ supercell. Our FPMD simulations were based on the canonical *N*-*V*-*T* ensemble with Nose thermostat, where *N* is the number of atoms, *V* is the volume, and *T* is the temperature. The initial structure for pure iron was melted at 8,000 K (or higher temperature for small volumes) and then quenched down to desired lower temperatures. Depending on temperature, different volume ranges between $V/V_0 = 1.06$ and 0.59 (where V_0 = 1728.0 Å^3 was used as a reference volume) were considered. At each thermodynamic state considered, the total pressure (*P*) represents the sum of the pressure obtained from the FPMD simulation, the ideal gas contribution given by NkT/V (where *k* is Boltzmann constant) and small Pulay stress of 0.4 to 0.8 GPa over the volume range considered. The run durations of our simulations ranged from 10 picoseconds at 7000 K to 20 picoseconds at 4000 K with a time step of 1 fs. For pure liquid iron, we also considered 2000 and 3000 K isotherms and additional volumes to cover the conditions at which experimental data are available for comparison (Kuwayama et al., 2020). A few simulations were performed along the 4000 K isotherm using the local density approximation to the exchange-correlation functional. For each simulated system, we

used the atomic-position time series to analyze local structure and speciation of the impurity elements. Selected simulations were run much longer to ensure that the calculated properties were well converged.

3. Results and Analysis

3.1 Equation of state

We first present and analyze the calculated pressure-volume-temperature results of pure iron liquid shown in Fig. 1. The pressure varies from 1.0 to 11.8 GPa at 2000 K, 1.9 to 90.3 GPa at 3000 K, 9.0 to 140.6 GPa at 4000 K, 15.5 to 270.0 GPa at 5000 K, 21.6 to 368.7 GPa at 6000 K, and 130.5 to 380.4 GPa at 7000 K for the respective volume ranges considered. These results are accurately described using the following relation:

$$P(V,T) = P(V,T_0) + B_{\text{th}}\,(T\text{-}T_0) \qquad (1)$$

Here the reference isotherm T_0 = 5000 K (first term) is described by the fourth-order Birch-Murnaghan equation of state with V_0 = 1728.0 Å^3 which corresponds to P_0 = 25.6 ± 0.3 GPa at 5000 K (shown by the black curve and circles in Fig. 1). The fit parameters are: K_0 = 196.2 ± 0.3 GPa, K_0' = 4.51 ± 0.06, and K_0'' = -0.026 ± 0.002 GPa^{-1}.

The thermal pressure P_{th} term contains the volume-temperature dependent coefficient:

$$B_{\text{th}}(V,T) = \left[0.0203 - 0.0132\left(\frac{V}{V_0}\right)\right]\left[0.9 + 0.1\left(\frac{T_0}{T}\right)\right] \qquad (2)$$

in the units of GPaK^{-1}. The model $P_{\text{th}} = B_{\text{th}}\,(T\text{-}T_0)$ describes well the values of thermal pressure calculated relative to 5000 K as a function of compression at different temperatures for pure and alloyed iron liquids (Fig. 2A). The two-term form of the equation of state (Eq. 1) gives root mean square error of 0.35 GPa for pure iron liquid thereby giving accurate representation over very wide ranges of pressure (0 to 400 GPa) and temperature (2000 to 7000 K).

We find that at the same volume and temperature conditions the calculated pressures for Ni- and Co-bearing liquids almost overlap with those for pure iron liquid lying within 0.8 GPa. However, the addition of Mo or W to liquid iron gives systematically higher pressure. The impurity-induced change in the pressure increases from about 2 to 17 GPa for Mo/W-bearing liquids over two-fold compression range considered (Fig. 2B). This finding is generally consistent with the notion that both Mo and W have larger atomic radii than iron radius. By adding an impurity-dependent term, we obtain the equation of state for iron-rich liquids as follows:

$$P(V,T) = P(V,T_0) + B_{\text{th}}\,(T\text{-}T_0) + B_{\text{im}}\,x \qquad (3)$$

Here x is the impurity concentration in atom% (equivalently, mol%) of iron-rich binary alloy liquid and B_{im} is a volume-dependent coefficient expressed as

$$B_{\mathrm{im}}(V) = a + b\left(\frac{V}{V_0}\right) + c\left(\frac{V}{V_0}\right)^2 \quad (4)$$

in the units of GPa per atom%. The parameters *a*, *b*, and *c* take small values, respectively, -0.13, 0.27, and 0 for $Fe_{146}Ni_4$ and -0.30, 0.42. and 0 for $F_{146}eCo_4$ liquid. Their respective values are 22.8, 40.8, and 18.8 for $Fe_{146}Mo_4$ and 27.1, -48.7, and 22.5 for $Fe_{146}W_4$ liquid. We find that the model $P_{\mathrm{im}} = B_{\mathrm{im}}\, x$ adequately describes the impurity-induced pressure values relative to pure iron liquid for x = 2.67 atom% (Fig. 2B). The model also works well for higher concentration as shown for the case of 5.33 atom% W-bearing iron liquid (Fig. S1). It is remarkable that the proposed three-term form of the equation of state (Eq. 3) accurately represents the calculated pressure-volume-temperature results for all iron-rich alloy systems (Fig. 3). The root mean square errors are 0.34, 0.29, 0.41, and 0.60 GPa, respectively, for Ni-, Co-, Mo- and W-bearing liquids. We find that the bulk modulus of iron-rich liquid remains essentially unchanged in the presence of any of these heavy elements (Fig. S2).

From the calculated temperature variations of the energy and pressure, we evaluate the heat capacity at constant volume and the thermal Grüneisen parameter using $C_V = \left(\frac{dE}{dT}\right)_V$ and $\gamma = \left(\frac{V}{C_V}\right)\left(\frac{dP}{dT}\right)_V$, respectively. Both C_V and γ are highly sensitive to pressure and some extent to temperature. The value of specific heat evaluated by assuming the linear temperature variation of energy at each volume in the range 4000 to 7000 K is constant with respect to temperature, but its value increases with compression (Fig. 4A). On the other hand, the value of γ evaluated assuming the linear temperature variation of thermal pressure at each volume in the same temperature range tends to increase somewhat initially with compression and then gradually decreases at higher pressures (Fig. 4B). The predicted behavior of C_V and γ is generally consistent with the previous calculations of iron liquid at high temperatures (Alfe et al., 2000; Bajgain et al., 2021). The calculated constant-temperature values of C_V and γ for all four alloys almost overlap with those of pure liquid iron (Fig. 4A, B). Thus, both thermodynamic parameters are essentially insensitive to the composition of iron-rich liquid for small impurity concentrations considered in this study (Fig. S1). Assuming a non-linear temperature variation for both energy and thermal pressure, we find that C_V does not show any systematic trend with temperature but γ slightly increases with deceasing temperature from 6500 K to 4500 K (Fig S3). They tend to take larger values as temperature is lowered further. For instance, the reference volume values of γ are 1.79 at 3500 K and 1.96 at 2500 K compared to the high-temperature average of 1.57. For pure and all iron alloy liquids, we generally find smaller gamma values at higher pressure (Fig. 4B). This implies a smaller temperature gradient in the deeper parts of the outer core.

3.2 Structural Properties

We analyze the structural properties of pure and alloyed iron liquids in terms of radial distribution functions and coordination environments. For pure iron liquid, the radial distribution

function shows characteristic features of a simple monoatomic liquid at all conditions (Fig. 5A and B). The calculated Fe-Fe RDF at low pressure shows a clear first peak at about 2.4 $Å^3$ corresponding to short-range order and subsequent smaller and broader peaks eventually converging to the unity implying the absence of long-range order. The first peak gets shorter and broader with increasing temperature whereas it becomes taller and sharper with increasing pressure (Fig. S4). The positions of both the first peak and the first minimum shift to shorter distance by about 0.3 and 0.5 Å, respectively, as the liquid is compressed from V/V_0 = 1.06 to 0.59 (Fig. S4). The predicted pressure-induced shifts are qualitatively consistent with the recent experimental inferences (Kuwayama et al., 2020).

For binary $Fe_{146}X_4$ liquids, we consider three partial radial distribution functions corresponding to the Fe-Fe, Fe-X, and X-X correlations. Irrespective of impurity type (X = Ni, Co, Mo, or W), the Fe-Fe RDF of all alloy liquids shows a well-defined peak which essentially overlaps with that of pure iron at all conditions. The X-Fe (equivalently, Fe-X) functions also show a clear first peak which is sensitive to both temperature and pressure. It is interesting to note that the Ni-Fe and Co-Fe functions closely resemble the Fe-Fe RDF with their first peaks almost overlapping with each other at all conditions (Fig. 5A). This means that both Co and Ni structurally behave as host iron atoms and can be considered iron-like as suggested previously for Ni-bearing iron alloy (Posner and Steinle- Neumann, 2019; Umemoto and Hirose, 2020). On the other hand, the Mo-Fe and W-Fe peaks are shifted to the right by about 0.2 Å (Fig. 5B). At a constant volume, the first peak of each X-Fe RDF becomes shorter and broader with its position shifting to shorter distance as temperature increased. Along a given isotherm, the peak becomes taller and sharper and systematically shifts to shorter distance as the liquid is compressed (Fig. S5). The minimum after the first peak gets deeper and shifts to shorter distance with compression but does not change noticeably with temperature. We find that the X-X RDF of each alloy liquid shows a weak peak at most conditions implying weak impurity-impurity correlation, so no direct bonds are formed among the impurity atoms (Fig S5). However, the Fe-Fe RDF of alloy liquid remains essentially unaffected by in the presence of the impurity element (Fig S6).

We calculate the average lengths of Fe-Fe and X-Fe (or Fe-X) bonds in all liquids from the first peak of the corresponding RDFs as a function of pressure and temperature. The average Fe-Fe distance is not affected significantly by the impurity at all conditions (Fig S7) as expected because of almost unaltered Fe-Fe RDF peak of each iron-rich alloy (Fig S6). The calculated average Ni-Fe and Co-Fe bond distances tend to be slightly larger (< 1%) than the Fe-Fe bond distance (Fig. 6). This prediction is consistent with the previous computational study of Ni-bearing liquid (Posner and Steinle-Neumann, 2019). In contrast, both Mo-Fe and W-Fe bonds are longer than Fe-Fe bonds by about 5 and 6%, respectively (Fig. 6). Wider RDF peaks and corresponding longer bond distances of Mo and W-bearing alloys can be related to the notion that Mo and W atomic radii are larger than the atomic radius of host iron, which is comparable to the radii of Ni and Co atoms.

For pure iron liquid, we examine local coordination environment involving multiple atoms which are the nearest neighbors of each atom. The mean Fe-Fe coordination number (Z_{FeFe}) is calculated by counting those iron atoms which lie within the cutoff distance corresponding to the minimum after the first peak of the radial distribution function. The calculated value of Z_{FeFe} is around 12.8 at low pressures and it tends to increase somewhat initially with compression and always remains below 13.5 at pressures up to ~400 GPa (Fig. 7A). The effects of temperature on coordination are small and do not show any discernable trend. Considering all thermodynamic states, we find that the mean Fe-Fe coordination number of liquid iron is somewhat larger than the coordination number of 12 for the cubic and hexagonal close-packed structures of solid iron. The liquid iron thus adopts a very dense structure of packing. At each condition, the coordination environment exhibits broad distribution consisting of 8-fold to 15-fold states in different proportions. As pressure increases, the coordination distribution shifts to higher values with increased proportions of 14 and 15-fold states at the expense of low coordination species (8- and 9-fold). The absence of low coordination states (below 8-fold) means that directional bonding is essentially absent in the liquid structure of iron.

We can define four types of coordination numbers for FeX alloy liquid: Z_{FeFe}, Z_{XFe}, Z_{FeX}, and Z_{XX}. Each alloying element tends to suppress the coordination among host iron atoms at all conditions. The reductions in Z_{FeFe} compared to pure liquid iron are in the range 2 to 4% for each binary iron alloy containing 2.67 atom % impurity (Fig. 7A). This means that the host atoms are also coordinated with some impurity atoms as first-nearest neighbors. All Fe-X coordination numbers are small (with Z_{FeX} taking values in the range 0.3 and 0.4) because majority iron atoms (~70%) are not bonded with any impurity atoms for the concentration considered here. The remaining Fe atoms are singly coordinated with X atoms, and the X-Fe-X connections occur in small proportion (below 5%). The sum of Z_{FeFe} and Z_{FeX} of each alloy liquid is almost equal to Z_{FeFe} of pure liquid iron.

The value of Z_{XFe} is sensitive to the type of alloying element (Fig. 7B). The mean iron coordination numbers of Ni and Co are the same as Z_{FeFe} of the alloy liquids but smaller than that of pure iron liquid. However, both Mo and W show higher Fe coordination with Z_{MoFe} and Z_{WFe} taking values between 13.5 and 15.0. The high mean Mo/W-Fe coordination numbers are consistent with longer Mo/W-Fe distances compared to Fe-Fe bonds. It is interesting to note that Z_{XFe} does not vary smoothly with compression. When the X-Fe coordination takes relatively small or large number, the impurity atoms tend to be correspondingly more or less correlated with each other. Unlike other types of coordination, we cannot define the X-X coordination precisely because of weak or no peak in the X-X RDFs. Using the respective X-Fe cutoff distances instead, we estimate Z_{XX} to lie between 0 and 1 considering all alloy liquids and all conditions. For instance, along the 5000 K, Z_{CoCo} = 0.8 and 0.0, respectively, when Z_{CoFe} is 12.5 and 13.4 so the total coordination number ($Z_{CoFe} + Z_{CoCo}$) of Co remains almost the same (13.3 and 13.4).

4. Discussion and implications

Our simulation of pure liquid iron covers the pressure range from 0 GPa at 2000 K to 380 GPa at 7000 K (Fig. 1). These results perhaps represent one of the most extensive studies of liquid iron when compared to many previous computational studies (e.g., Alfe et al., 2000; Ichikawa et al., 2014; Wagle and Steinle-Neumann, 2019; Umemoto and Hirose, 2020; Bajgain et al., 2021) and they are expected to give additional insight onto the thermodynamic behavior of liquid iron. Unlike the case of silicate melts (e.g., Karki et al., 2018), the first-principles computations tend to overestimate the liquid iron density (or underestimate the volume) considerably even with the use of GGA. As such, the differences between the calculated and experimental values of liquid iron density are large as previously noted by most previous computational studies. Accurate evaluation of the liquid density is needed to infer meaningful constraints on the composition of the Earth's outer core from density comparisons between iron-rich alloys and seismological observations. Towards this endeavor, appropriate corrections need to be made to the calculated results by considering their systematic offset from the available experimental data. We find that the calculated densities of liquid iron are higher than the measured data at zero pressure and all elevated pressures up to 116 GPa in the temperature range 1800 to 4350 K of the experimentation (Kuwayama et al., 2020). This apparent overestimation of the density by our first-principles computation ($\Delta\rho = \rho_{\mathrm{calc}} - \rho_{\mathrm{expt}}$) is ~1.1 g/cc at zero pressure and 2000 K. The value of $\Delta\rho$ decreases with increasing pressure to about 0.4 g/cc around 110 GPa and 4300 K. These density differences correspond to finite differences in pressure between computation and experiments as GGA systematically underestimates the pressure. Comparison with the shock-wave density data available at pressures above 270 GPa does not seem to be appropriate in this regard because temperature in the shock-wave experiments is model dependent (Anderson and Ahrens, 1994). So, we use the experimental data at pressures 0 to 116 GPa only as the reference to derive an empirical pressure correction term as a function of compression (Inset of Fig. 8):

$$P_{\mathrm{emp}}(V) = P_{\mathrm{expt}}(V) - P_{\mathrm{calc}}(V) = 27 - 12\left(\frac{V}{V_0}\right) \quad (5)$$

This pressure correction is generally consistent with the previous corrections based on thermodynamics using the differences in both pressure and bulk modulus at zero pressure between computations and experiments (Wagle and Steinle-Neumann, 2019; Bajgain et al., 2021). Our correction model which is based on direct comparisons with the measured data at zero and elevated pressures is expected to be widely applicable than previous models. We find that using the local density approximation (LDA) further underestimates the pressure (Fig. 1) thus requiring even larger correction to the pressure.

The derived density-pressure profiles of pure liquid iron with the corrected pressure along all high-temperature isotherms (Fig. 8) lie systematically above the seismic density profile of the core (Dziewonski and Anderson, 1981). We also calculated the density profile along the isentropic temperature profile given by Kuwayama et al. (2020) with the inner core boundary temperature constrained at 5800 K (Fig. 8). It is thus clear that liquid iron is too dense for the outer core

composition. This notion has been established based on numerous experimental and computational studies, but the size of the density gap (or density deficient) is not well constrained. Based on our corrected equation of state, the density gap varies from 0.68 to 0.82 g/cc (that is, 6.9 to 6.7%) from the top to the bottom of the outer core, which are smaller than most previous estimates by 1 to 2% and comparable to the most recent inferences (Kuwayama et al., 2020). Based on the calculated density results (Fig. 9), the addition of Ni and Co in a few atom% does not change the density of iron-rich liquids at all. As such, these elements are invisible in the outer core with respect to the seismic density and velocity observations. However, other two heavy elements, particularly W, in any amounts tends to increase the density of iron-rich liquid (Fig. 9) thereby widening the density gap. For instance, the addition of 0.1 atom% of W increases the liquid density by ~0.02 g/cc which can be offset by the addition of about 10 times more hydrogen. This means that the estimation of the amounts of light elements in the outer core also depends on the presence of heavy elements even in fairly small amounts.

Our structural analysis shows that each of impurity elements (Ni, Co, Mo, and W) is incorporated in the liquid iron by substitutional mechanism. These impurity atoms adopt similar local structures like host iron atoms thereby taking close-pack positions. Moreover, visualization of the position-time series data reveals the presence of only transient structures consisting of two or rarely three impurity atoms bonded together. This means that the impurity atoms are less likely to form large clusters to be exsolved but instead they are compatible in the liquid iron by preferably bonding with the host atoms. We argue that iron-rich metallic liquid can dissolve any of these impurity elements in significant amounts under the pressure-temperature conditions that are relevant to the core formation time and to the present core. In the core formation model based on accreting impacting planetesimals, the iron-rich metal in each impactor may have interacted with the magma ocean and been molten (Wood et al., 2006). Metallic droplets from those impactors sank through the silicate magma ocean and siderophile elements could have then been carried down into the core along as the dissolved components (Kleine et al., 2002; Rubie et al., 2003). The amount of these elements carried to the core depends on their partitioning coefficients between the metallic liquid and silicate melts, and their diffusion rates. Our finding of structural similarity in the speciation of Mo and W in liquid iron supports the notion that these refractory siderophile elements show similar partitioning behavior (Huang et al., 2021). In the early stages of the Earth's core-mantle differentiation, these elements could have segregated to metallic liquid droplets. Such Mo- and W-bearing droplets (and metallic diapirs in the later stages) being excessively heavy could have sunk to the core. It is thus possible that the heavy elements may have been mostly collected to the bottommost part (referred to as the F-layer) which is distinct from the rest of the outer core (Zou et al., 2008).

5. Conclusions

Unlike liquid iron-light elements mixtures, the incorporation of heavy siderophile elements in liquid iron has not been studied much using first-principles computation. This study reports the computational results for four molten iron-rich alloys corresponding to 2.67 atom% of Ni, Co, Mo, and W at pressures up to 380 GPa and at temperatures 4000 to 7000 K using generalized gradient approximation. It is remarkable that a three-term form of the equation of state consisting of the reference pressure-volume isotherm $P(V,T_0)$, thermal pressure $B_{th}(T-T_0)$, and impurity pressure $B_{im}x$ accurately describes the calculated pressure-temperature-volume (P-V-T) results of all liquids. Moreover, the pressure is corrected for the apparent overestimation of liquid iron density relative to the recently reported high-pressure experimental data by adding the fourth term P_{emp} to the equation of state. The resulting density-pressure profile of pure iron liquid along a geotherm shows that the outer core suffers from a density deficient of ~ 6.8%, which is lower than most previous estimates by 1 to 2%. Our results show that the addition of Mo and W in liquid iron in any amount widens the density gap. Both Ni and Co do not affect the liquid density significantly and they almost behave as host iron atoms showing similar bond distances and local coordination. The mean lengths of Fe/Ni/Co-Fe bonds decrease from ~2.6 to ~2.15 Å and the mean Fe/Ni/Co-Fe coordination numbers increase from ~12.5 to ~13.5 over the entire pressure range considered. On the other hand, Mo and W show notable differences: The Mo/W-Fe bonds are longer than the Fe-Fe bonds by 5-6% and correspondingly, the mean iron coordination numbers of Mo/W atoms are higher than the mean Fe-Fe coordination numbers by 10-15%. All X-Fe and Fe-Fe coordination numbers thus exceed but remain close to 12. This means that the impurity atoms are incorporated via substitutional mechanism thus taking close-pack positions of iron atoms. In each alloy, impurity atoms are also found to be mostly non-interacting with each other and do not tend to form clusters. Based on these results, we suggest that each of these heavy elements is soluble in liquid iron in significant amount and may have facilitated core-mantle differentiation during the accretion phase. To constrain the amounts of these siderophile elements in the outer core requires more quantitative information about their behavior, including the diffusion rates and partitioning coefficients between silicate melts and metallic liquid.

Acknowledgements

The research was supported by NASA (80NSSC21K0377) and NSF (EAR 1463807). High computing resources were provided by Louisiana State University.

Appendix A. Supplementary material

Supplementary material related to this article is included.

References

Alfè, D., Kresse, G. and Gillan, M.J., 2000. Structure and dynamics of liquid iron under Earth's core conditions. Phys. Rev. B 61, 132-142.

Anderson, W.W., Ahrens, T.J., 1994. An equation of state for liquid iron and implications for the Earth's core. J. Geophys. Res. 99, 4273–4284.

Assael, M.J., Kakosimos, K., Banish, R.M., Brillo, J., Egry, I., Brooks, R., Quested, P.N., Mills, K.C., Nagashima, A., Sato, Y., and Wakeham, W.A., 2006. Reference data for the density and viscosity of liquid aluminum and liquid iron. J. Phys. Chem. Ref. Data 35, 285-300.

Badro, J., Coté, A.S., Brodholt, J.P., 2014. A seismologically consistent compositional model of Earth's core. Proc. Natl. Acad. Sci. 111, 7542–7545.

Bajgain, S.K., Mookherjee, M., and Dasgupta, R., 2021. Earth's core could be the largest terrestrial carbon reservoir. Comm. Earth Environ. 2, 165.

Brown, J.M., McQueen, R.G., 1986. Phase transitions, Grün isen parameter, and elasticity for shocked iron between 77 GPa and 400 GPa. J. Geophys. Res. 91, 7485–7494.

Dziewonski, A.M. and D.L. Anderson, 1981. Preliminary reference Earth model. Phys. Earth Planet. Inter. 25, 297-356.

Fei, Y. and Brosh, E., 2014. Experimental study and thermodynamic calculations of phase relations in the Fe–C system at high pressure. Earth Planet. Sci. Lett. 408, 155–162.

Fischer, R.A., Nakajima, Y., Campbell, A.J., Frost, D.J., Harries, D., Langenhorst, F., Miyajima, N., Pollok, K., Rubie, D.C., 2015. High pressure metal–silicate partitioning of Ni, Co, V, Cr, Si, and O. Geochim. Cosmochim. Acta 167, 177–194.

Hirose, K., Labrosse, S., Hernlund, J., 2013. Composition and state of the core. Annu. Rev. Earth Planet. Sci. 41, 657–691.

Huang, D., Siebert, J., and Badro J., 2021. High pressure partitioning behavior of Mo and W and late sulfur delivery during Earth's core formation. Geochim. Comochim. Acta 210, 19-31.

Ichikawa, H., Tsuchiya, T., Tange, Y., 2014. The P-V-T equation of state and thermodynamic properties of liquid iron. J. Geophys. Res., Solid Earth 119, 240–252.

Ichikawa, H. and Tsuchiya, T., 2020. Ab Initio thermoelasticity of liquid iron-nickel-light element alloys. Minerals 10, 59.

Karki, B.B., Ghosh, D.B., Maharjan, C., Karato, S-i, Park, J., 2018. Density-pressure profiles of Fe-bearing $MgSiO_3$ liquid: effects of valence and spin states, and implications for the chemical evolution of the lower mantle. Geophys. Res. Lett. 45, 3959–3966.

Kleine, T., Mün k r, C., Metzger, K., and Palme, H. (2002). Rapid accretion and early core formation on asteroids and the terrestrial planets from Hf- W chronometry. Nature 418, 952–955.

Kresse, G., Furthmü ller, J., 1996. Efficient iterative schemes for ab initio total-energy calculations using a plane-wave basis set. Phys. Rev. B54, 11169–11186.

Kuwayama, Y., Morard, G., Nakajima, Y., Hirose, K., Baron, A.Q.R., Kawaguchi, S.I., Tsuchiya, T., Ishikawa, D., Hirao, N., and Ohishi, Y., 2020. Equation of state of liquid iron under extreme conditions. Phys. Rev. Lett. 124, 165701.

McDonough, W.F. and Sun, S.s., 1995. The composition of the Earth. Chem. Geol. 120, 223-253.

Morard, G., Siebert, J., Andrault, D., Guignot, N., Garbarino, G., Guyot, F., Antonan-geli, D., 2013. The Earth's core composition from high pressure density measurements of liquid iron alloys. Earth Planet. Sci. Lett. 373, 169–178.

Perdew, J.P., Burke, K., Ernzerhof, M., 1996. Generalized gradient approximation made simple. Phys. Rev. Lett. 77, 3865–3868.

Poirier, J.P., 1994. Light elements in the Earths outer core: a critical review. Phys. Earth Planet. Inter. 85, 319–337.

Posner, E.S. and Steinle-Neumann, G., 2019. Mass transport and structural properties of binary liquid iron alloys at high pressure. Geochem. Geophys. Geosys. 20, 3556-3568.

Rubie, D.C., Melosh, H. J., Reid, J. E., Liebske, C. and Righter, K., 2003. Mechanisms of metal–silicate equilibration in the terrestrial magma ocean. Earth Planet. Sci. Lett. 205, 239-255.

Sakamaki, K., Takahashi, E., Nakajima, Y., Nishihara, Y., Funakoshi, K., Suzuki, T., Fukai, Y., 2009. Melting phase relation of FeH_x up to 20 GPa: implication for the temperature of the Earth's core. Phys. Earth Planet. Inter. 174, 192–201.

Tagawa, S., Sakamoto, N., Hirose, K., Yokoo, S., Hernlund, J., Ohishi, Y., Yurimoto, H., 2021. Experimental evidence for hydrogen incorporation into Earth's core. Nature Comm. 12, 2588.

Samuel, H., 2012. A re- evaluation of metal diapir breakup and equilibration in terrestrial magma oceans. Earth Planet. Sci. Lett. 313, 105–114.

Umemoto, K., Hirose, K., 2015. Liquid iron-hydrogen alloys at outer core conditions by first-principles calculations. Geophys. Res. Lett. 42, 7513–7520.

Umemoto, K. and Hirose, K., 2020. Chemical compositions of the outer core examined by first principles calculations. Earth Planet. Sci. Lett. 531, 116009.

Wagle, F., Steinle-Neumann, G., 2019. Liquid iron equation of state to the terapascal regime from ab initio simulations. J. Geophys. Res. 124, 3350–3364.

Wood, B.J., Walter, M.J., and Wade, J., 2006. Accretion of the Earth and segregation of its core. Nature 441, 825-833.

Zou, Z., Koper, K.D., Cormier, V. F., 2008. The structure of the base of the outer core inferred from seismic waves diffracted around the inner core. J. Gephys. Res. 113, B05314.